JEM Journal of Experimental Medicine

ARTICLE

# Dominant-negative mutations in human *IL6ST* underlie hyper-IgE syndrome

Vivien Béziat[1,2,3], Simon J. Tavernier[4,5*], Yin-Huai Chen[6,7*], Cindy S. Ma[8,9*], Marie Materna[1,2], Arian Laurence[6,7], Jens Staal[5], Dominik Aschenbrenner[6,7], Lisa Roels[4], Lisa Worley[8,9], Kathleen Claes[10], Lisa Gartner[6,7], Lisa A. Kohn[11], Marieke De Bruyne[10], Klaus Schmitz-Abe[12,13,14], Louis-Marie Charbonnier[15,16], Sevgi Keles[17], Justine Nammour[1,2], Natasha Vladikine[1,2], Majistor Raj Luxman Maglorius Renkilaraj[1,2], Yoann Seeleuthner[1,2], Mélanie Migaud[1,2], Jérémie Rosain[1,2], Mohamed Jeljeli[18], Bertrand Boisson[1,2,3], Eva Van Braeckel[19], Jill A. Rosenfeld[20], Hongzheng Dai[20], Lindsay C. Burrage[20], David R. Murdock[20], Bart N. Lambrecht[21,22], Véronique Avettand-Fenoel[23], Tiphanie P. Vogel[24], Undiagnosed Diseases Network, Charles R. Esther Jr.[25], Sule Haskologlu[26], Figen Dogu[26], Peter Ciznar[27], David Boutboul[28], Marie Ouachée-Chardin[29], Jean Amourette[30], Marie-Noëlle Lebras[31], Clément Gauvain[32], Colas Tcherakian[33], Aydan Ikinciogullari[26], Rudi Beyaert[5], Laurent Abel[1,2,3], Joshua D. Milner[34,35], Bodo Grimbacher[36,37,38,39,40], Louis-Jean Couderc[33,41], Manish J. Butte[11**], Alexandra F. Freeman[34**], Émilie Catherinot[33**], Claire Fieschi[28,42**], Talal A. Chatila[15,16**], Stuart G. Tangye[8,9***], Holm H. Uhlig[6,7***], Filomeen Haerynck[4,43***], Jean-Laurent Casanova[1,2,3,44,45***], and Anne Puel[1,2,3***]

**Autosomal dominant hyper-IgE syndrome (AD-HIES) is typically caused by dominant-negative (DN) *STAT3* mutations. Patients suffer from cold staphylococcal lesions and mucocutaneous candidiasis, severe allergy, and skeletal abnormalities. We report 12 patients from 8 unrelated kindreds with AD-HIES due to DN *IL6ST* mutations. We identified seven different truncating mutations, one of which was recurrent. The mutant alleles encode GP130 receptors bearing the transmembrane domain but lacking both the recycling motif and all four STAT3-recruiting tyrosine residues. Upon overexpression, the mutant proteins accumulate at the cell surface and are loss of function and DN for cellular responses to IL-6, IL-11, LIF, and OSM. Moreover, the patients' heterozygous leukocytes and fibroblasts respond poorly to IL-6 and IL-11. Consistently, patients with *STAT3* and**

[1]Laboratory of Human Genetics of Infectious Diseases, Necker Branch, Institut National de la Santé et de la Recherche Médicale (INSERM) U1163, Paris, France; [2]University of Paris, Imagine Institute, Paris, France; [3]St. Giles Laboratory of Human Genetics of Infectious Diseases, Rockefeller Branch, The Rockefeller University, New York, NY; [4]Primary Immune Deficiency Research Laboratory, Department of Internal Diseases and Pediatrics, Centre for Primary Immunodeficiency Ghent, Jeffrey Modell Diagnosis and Research Centre, Ghent University Hospital, Ghent, Belgium; [5]VIB-UGent Center for Inflammation Research, Unit of Molecular Signal Transduction in Inflammation, Ghent, Belgium; [6]Translational Gastroenterology Unit, John Radcliffe Hospital, University of Oxford, Oxford, UK; [7]Department of Paediatrics, University of Oxford, Oxford, UK; [8]Immunology Division, Garvan Institute of Medical Research, Darlinghurst, Sydney, New South Wales, Australia; [9]St. Vincent's Clinical School, UNSW Sydney, Sydney, New South Wales, Australia; [10]Center for Medical Genetics, Ghent University Hospital, Ghent, Belgium; [11]Division of Immunology, Allergy, and Rheumatology, Department of Pediatrics, University of California, Los Angeles, Los Angeles, CA; [12]Division of Newborn Medicine and Neonatal Genomics Program, Boston Children's Hospital, Harvard Medical School, Boston, MA; [13]Division of Genetics and Genomics, Boston Children's Hospital, Harvard Medical School, Boston, MA; [14]The Manton Center for Orphan Disease Research, Boston Children's Hospital, Harvard Medical School, Boston, MA; [15]Department of Pediatrics, Harvard Medical School, Boston, MA; [16]Division of Immunology, Boston Children's Hospital, Boston, MA; [17]Necmettin Erbakan University, Meram Medical Faculty, Division of Pediatric Allergy and Immunology, Konya, Turkey; [18]Cochin University Hospital, Biological Immunology Unit, Assistance Publique Hôpitaux de Paris (AP-HP), Paris, France; [19]Department of Respiratory Medicine, Ghent University Hospital, Ghent Belgium; [20]Department of Molecular and Human Genetics, Baylor College of Medicine, Houston, TX; [21]VIB-UGent Center for Inflammation Research, Unit of Immunoregulation and Mucosal Immunology, Ghent, Belgium; [22]Department of Internal Medicine and Pediatrics, Ghent University, Ghent, Belgium; [23]Laboratory of Clinical Microbiology, Virology Unit, Necker Hospital for Sick Children, AP-HP, Paris, France; [24]Division of Rheumatology, Department of Pediatrics, Baylor College of Medicine and Texas Children's Hospital, Houston, TX; [25]Pediatric Pulmonology, University of North Carolina at Chapel Hill, Chapel Hill, NC; [26]Division of Pediatric Immunology and Allergy, Ankara University School of Medicine, Sıhhıye, Ankara, Turkey; [27]Department of Pediatrics, Faculty of Medicine Comenius University and Children's University Hospital, Bratislava, Slovakia; [28]Clinical Immunology Department, Saint Louis Hospital, AP-HP de Paris University of Paris, Paris, France; [29]Department of Pediatric Hematology and Immunology, Robert Debré Hospital, AP-HP, Paris, France; [30]Pulmonology Department, Centre Hospitalier d'Arras, Arras, France; [31]Pediatric Pulmonology, Infectious Disease and Internal Medicine Department, AP-HP, Robert Debré Hospital, Paris, France; [32]Thoracic Oncology Department, Lille University Hospital, Lille, France; [33]Hôpital Foch, Pulmonology Department, Suresnes, France; [34]National Institute of Allergy and Infectious Diseases, Bethesda, MD; [35]Division of Allergy, Immunology and Rheumatology, Department of Pediatrics, Columbia University Irving Medical Center, New York, NY; [36]Institute for Immunodeficiency, Center for Chronic Immunodeficiency, Medical Center, Faculty of Medicine, Albert Ludwig University of Freiburg, Freiburg, Germany; [37]German Center for Infection Research, Satellite Center Freiburg, Freiburg, Germany; [38]Centre for Integrative Biological Signaling Studies, Albert Ludwig University, Freiburg, Germany; [39]RESIST, Cluster of Excellence 2155 to Hanover Medical School, Satellite Center Freiburg, Freiburg, Germany; [40]Institute of Immunity and Transplantation, Royal Free Hospital, University College London, London, UK; [41]Simone Veil Faculty of Life Sciences, Versailles-Paris Saclay University, UPRES EA-220, Suresnes, France; [42]INSERM UMR1126, Institut de Recherche Saint-Louis, Université de Paris, Paris, France; [43]Department of Internal Medicine and Pediatrics, Division of Pediatric Immunology and Pulmonology, Ghent University Hospital, Ghent, Belgium; [44]Pediatric Hematology-Immunology Unit, Necker Hospital for Sick Children, AP-HP, Paris, France; [45]Howard Hughes Medical Institute, New York, NY.

Members of the Undiagnosed Diseases Network are listed in Data S1. *S.J. Tavernier, Y.-H. Chen, and C.S. Ma contributed equally to this paper; **M.J. Butte, A.F. Freeman, É. Catherinot, C. Fieschi, and T.A. Chatila contributed equally to this paper; ***S.G. Tangye, H.H. Uhlig, F. Haerynck, J.-L. Casanova, and A. Puel contributed equally to this paper; Correspondence to Jean-Laurent Casanova: jean-laurent.casanova@rockefeller.edu; Vivien Béziat: vivien.beziat@inserm.fr.

**_IL6ST_ mutations display infectious and allergic manifestations of IL-6R deficiency, and some of the skeletal abnormalities of IL-11R deficiency. DN _STAT3_ and _IL6ST_ mutations thus appear to underlie clinical phenocopies through impairment of the IL-6 and IL-11 response pathways.**

## Introduction

Job's syndrome was first described in 1966 in patients with recurrent "cold" staphylococcal abscesses, eczema, and respiratory infections (Davis et al., 1966). In 1972, high serum IgE levels were found in patients with this condition, which was then renamed hyper-IgE syndrome (HIES; Buckley et al., 1972; Zhang et al., 2018b; Bergerson and Freeman, 2019; Buckley, 2020). These patients also often have eosinophilia, low levels of inflammatory markers during infection, chronic mucocutaneous candidiasis (CMC), and extrahematopoietic disorders, including skeletal lesions in particular (e.g., deciduous tooth retention, osteopenia, and scoliosis; Grimbacher et al., 1999a; Chandesris et al., 2012a). HIES is typically inherited as an autosomal dominant (AD) trait (Grimbacher et al., 1999a). Disease-causing monoallelic DN missense variations of the gene encoding signal transducer and activator of transcription 3 (*STAT3*) were first reported in 2007 in patients with the full HIES phenotype (Minegishi et al., 2007). Over 100 different rare variants of *STAT3* have since been reported (Holland et al., 2007; Renner et al., 2007; Chandesris et al., 2012b; Vogel et al., 2015; Khourieh et al., 2019). In some kindreds, typical HIES segregates as an autosomal recessive (AR) trait (AR-HIES). Some patients with AR-HIES carry biallelic null mutations of the zinc-finger 341 gene (*ZNF341*), encoding a transcription factor governing basal and inducible STAT3 expression (Béziat et al., 2018; Frey-Jakobs et al., 2018). AR DOCK8 and PGM3 deficiencies and AD CARD11 deficiency are not genetic etiologies of bona fide HIES, as affected patients have high serum IgE levels and eczema in the context of clinical manifestations not seen in ZNF341 and STAT3 deficiencies and lack many clinical phenotypes of these deficiencies, including weak inflammation and characteristic extrahematopoietic disorders (Zhang et al., 2009, 2014, 2018b; Engelhardt et al., 2009; Sassi et al., 2014; Ma et al., 2017).

STAT3 is a signaling molecule acting downstream of many cytokine receptors, such as IFNAR1, IL-6R, IL-10R, IL-11R, IL-21R, IL-22R, IL-23R, oncostatin M (OSM)–R, and leukemia inhibitory factor (LIF)–R; Kane et al., 2014). The multisystemic nature of the clinical phenotypes seen in AD-HIES patients probably reflects this pleiotropy. Complete *Stat3* deficiency is embryonic lethal in mice (Takeda et al., 1997). However, AD-HIES patients retain residual STAT3 activity, and mice with DN germline mutations of *Stat3* and a similar degree of residual STAT3 activity are born healthy (Steward-Tharp et al., 2014). These mice have high levels of IgE expression and are susceptible to bacterial infection but do not fully reproduce the HIES phenotype, making it difficult to decipher the pathogenesis of individual human HIES phenotypes. By contrast, the progressive identification of human inborn errors of cytokines or of their receptors signaling through STAT3 have clarified several HIES phenotypes. Some related deficiencies do not have phenotypes overlapping with HIES. Patients with IL-23R deficiency suffer from isolated mycobacteriosis (Martínez-Barricarte et al., 2018), patients with IL-10RA or IL-10RB deficiency suffer from inflammatory bowel disease (Glocker et al., 2011; Kotlarz et al., 2012; Moran et al., 2013), and patients with IFNAR1 or IFNAR2 deficiency suffer from severe viral infections (Duncan et al., 2015; Hernandez et al., 2019). Other deficiencies overlap with HIES. Patients with IL-21 or IL-21R deficiency share some of the features of HIES, with high serum IgE concentrations, recurrent respiratory infections, and impaired humoral immune responses. However, unlike HIES patients, they also display severe cryptosporidiosis (Kotlarz et al., 2013, 2014; Salzer et al., 2014; Erman et al., 2015; Stepensky et al., 2015). Patients with IL-11RA deficiency suffer from craniosynostosis and dental abnormalities, without significant immunodeficiency (Nieminen et al., 2011). Patients with LIF-R deficiency develop Stüve-Wiedemann syndrome (SWS), a multisystem disorder characterized by profound bone defects and disordered respiratory, cardiac, and autonomic nervous systems (Dagoneau et al., 2004). These patients also develop scoliosis, osteoporosis, and dental abnormalities. Few patients with SWS survive the neonatal period. Patients with partial OSM-R deficiency develop pruritus and cutaneous amyloidosis (Arita et al., 2008). Patients with complete IL-6R deficiency develop recurrent skin and lung infections, eczema, high IgE levels, abnormal acute-phase responses, and eosinophilia (Spencer et al., 2019; Puel and Casanova, 2019).

*IL6ST* encodes GP130, a signaling receptor subunit used by all IL-6 family cytokines, including IL-6, IL-11, IL-27, LIF, OSM, IL-35, cardiotrophin-1, cardiotrophin-like cytokine, and ciliary neurotrophic factor (Rose-John, 2018). In mice, complete GP130 deficiency is lethal in utero due to myocardial, hematological, and skeletal defects, reflecting the pleiotropic role of this molecule (Yoshida et al., 1996; Kawasaki et al., 1997). A condition similar to SWS, with skeletal malformations, respiratory failure, and perinatal death, was recently reported in fetuses and patients homozygous for loss-of-function (LOF) mutations in *IL6ST* (Monies et al., 2019; Chen et al., 2020). By contrast, patients with AR partial, as opposed to complete, GP130 deficiency present recurrent lung infections, eczema, eosinophilia, high serum IgE levels, impaired acute-phase responses, craniosynostosis, scoliosis, and deciduous tooth retention (Schwerd et al., 2017; Shahin et al., 2019). The proximal cytoplasmic region of GP130 contains two boxes that constitutively bind JAKs (Lütticken et al., 1994). Upon cytokine activation, JAKs phosphorylate tyrosine residues 767, 814, 905, and 915 in the cytoplasmic domain of GP130, leading to the recruitment and activation of STAT1, STAT3, and, to a lesser extent, STAT5 (Lütticken et al., 1994; Hunter and Jones, 2015; Murakami et al., 2019). No known cytokine can activate GP130 in the absence of another receptor chain. IL-6 and IL-11 first bind IL-6R and IL-11R, respectively, forming a hexameric complex with GP130 with a valence of 2:2:2 (Murakami et al., 1993; Barton et al., 2000). IL-27, LIF, and OSM use IL-27RA, LIF-R, and OSM-R, respectively, to form a heterotrimer with

GP130 (Gearing et al., 1992; Mosley et al., 1996; Pflanz et al., 2004). IL-6R and IL-11R cannot signal through their own intracellular domains. Consequently, these cytokines rely on GP130 for their function. By contrast, IL-27RA, LIF-R, and OSM-R can recruit STATs via specific motifs present in their intracellular domains.

In this context, the less severe outcome of patients with AR partial GP130 deficiency than of those with AR complete GP130 deficiency can be explained by the apparently largely intact LIF signaling and impaired, but not abolished, IL-6, IL-11, IL-27, and OSM signaling (Schwerd et al., 2017; Shahin et al., 2019; Monies et al., 2019; Chen et al., 2020). No deficiencies of IL-27RA or ciliary neurotrophic factor receptor have been described, but most of the immunological and extrahematopoietic phenotypes of patients with AR partial or complete GP130 deficiency have been seen in patients lacking IL-6R, IL-11R, LIF-R, or OSM-R deficiency (Schwerd et al., 2017; Shahin et al., 2019; Spencer et al., 2019; Nieminen et al., 2011; Mikelonis et al., 2014; Arita et al., 2008). Collectively, these findings suggest that many, perhaps even most, of the immunological abnormalities seen in patients with STAT3 deficiency, whether biological (high IgE levels), clinical (atopy and recurrent staphylococcal infections), or both (low levels of inflammation), are due to poor cellular responses to IL-6 (Puel and Casanova, 2019), whereas most of the skeletal abnormalities are due to poor responses to IL-11 (craniosynostosis and deciduous tooth retention) or LIF (scoliosis, osteoporosis). The apparent lack of CMC in patients with AR deficiency of IL-6R, IL-10RA, IL-10RB, IL-11R, IL-21R, IL-23R, IFNAR1, IFNAR2, LIF-R, or OSM-R deficiency (Schwerd et al., 2017; Spencer et al., 2019; Nieminen et al., 2011; Mikelonis et al., 2014; Arita et al., 2008; Martínez-Barricarte et al., 2018; Hernandez et al., 2019; Glocker et al., 2011; Kotlarz et al., 2014; Duncan et al., 2015) also suggested that the pathogenesis of impaired IL-17 immunity and CMC in patients with mutations in STAT3 or ZNF341 may involve the disruption of multiple cytokine responsive pathways (Minegishi et al., 2007; Puel et al., 2011; Béziat et al., 2018; Ma et al., 2016). We tested whether new genetic etiologies of AD-HIES could shed light on the pathogenesis of various individual HIES phenotypes.

## Results

### Rare monoallelic *IL6ST* variants in HIES patients

We investigated 12 patients with HIES from 8 unrelated families of French (kindreds A and B), Bulgarian (kindred C), Slovakian (kindred D), American (kindreds E, G, and H), or Turkish (kindred F) origin (Fig. 1, A and B; and Table S1). With the exception of the parents of P6 (kindred C), who were second cousins, none of the patients were known to be the fruit of consanguineous unions. This presence or absence of consanguinity was confirmed by the high or low percentage of homozygosity on whole-exome sequencing (WES) in five patients (P2, P3, and P4 = 0.17%, P5 = 0.28%, and P6 = 2.0%). In kindreds A and C, the HIES phenotype was observed in several consecutive generations of affected male and female individuals, consistent with segregation as an AD trait. The other patients (P5 and P8–P12) had no family history of HIES. Mutations of *STAT3* were excluded in the first two kindreds identified by targeted sequencing of all exons and sequencing the full-length cDNA of P2 (kindred A) and P5 (kindred B). We performed WES for 10 patients. No candidate mutations were found in known HIES-causing and other primary immunodeficiency genes, including *ZNF341*, *IL6R*, *DOCK8*, *TYK2*, *PGM3*, and *STAT3*. By contrast, all 10 patients carried a heterozygous stop codon or frameshift mutation in *IL6ST* (Fig. 1, A and C). P2, P3, and P4 (kindred A) carried a heterozygous duplication of 5 nt (c.2277_2281dup) resulting in a frameshift followed by a premature stop codon 29 amino acids downstream (p.T761Ifs*29, subsequently abbreviated to T761fs; Fig. 1, A and C). P5 (kindred B) and P6 (kindred C) carried the same heterozygous duplication of one adenine residue (c.2155dup), resulting in a frameshift and a premature stop codon two amino acids downstream (p.I719Nfs*2, subsequently abbreviated to I719fs; Fig. 1, A and C). P8 (kindred D) carried a heterozygous substitution of 1 nt (c.2199C>A), resulting in a premature stop codon (p.C733*; Fig. 1, A and C). P9 (kindred E) carried a heterozygous deletion of one thymidine residue (c.2121del), resulting in a frameshift followed immediately by a premature stop codon (p.L708*; Fig. 1, A and C). P10 (kindred F) carried a heterozygous substitution of one nucleotide (c.2277T>G), resulting in a premature stop codon (p.Y759*; Fig. 1, A and C). P11 (kindred G) carried a heterozygous duplication of one thymidine residue (c.2224dup), resulting in a frameshift and a premature stop codon two amino acids downstream (p.S742Ffs*2, subsequently abbreviated to S742fs; Fig. 1, A and C). P12 (kindred H) carried a heterozygous substitution of 1 nt (c.2261C>A), resulting in a premature stop codon (p.S754*; Fig. 1, A and C). Sanger sequencing confirmed the mutations in all eight kindreds, and confirmed that P7 was heterozygous for the p.I719fs. The familial segregation patterns of the mutant alleles were consistent with an AD trait with full penetrance (Fig. 1 A). The mutations in P5 (c.2155dup), P9 (c.2121del), P10 (c.2277T>G), and P11 (c.2224dup) had occurred de novo. The c.2155dup, which occurred in two unrelated families, is therefore recurrent not because of a founder effect but probably due to a mutational hotspot. None of the seven mutations was reported in any public database (Bravo, gnomAD v2.1, and ClinVar). All mutations were predicted to be highly deleterious, with combined annotation-dependent depletion scores of 29.7, 27.0, 40.0, 26.3, 35.0, 33.0, and 40.0, respectively, well above the mutation significance cutoff of 3.3 (99% confidence interval) for *IL6ST* (Itan et al., 2016). All these *IL6ST* variants clustered in the intracellular C-terminal region (Fig. 1 C). All the mutated alleles were predicted to encode receptors that (1) reached the cell surface, as the premature stop codon was downstream from the transmembrane domain; (2) accumulated at the cell surface, due to the truncation of the STQPLL recycling motif (Dittrich et al., 1996); and (3) were LOF, due to the truncation of the four STAT3-docking sites (Stahl et al., 1995). This triad of features is strikingly similar to that of DN mutations of *IFNGR1* (Jouanguy et al., 1999), suggesting that these *IL6ST* mutations may be DN and pathogenic. Consistent with this hypothesis, truncated forms of mouse and human GP130 retaining cell

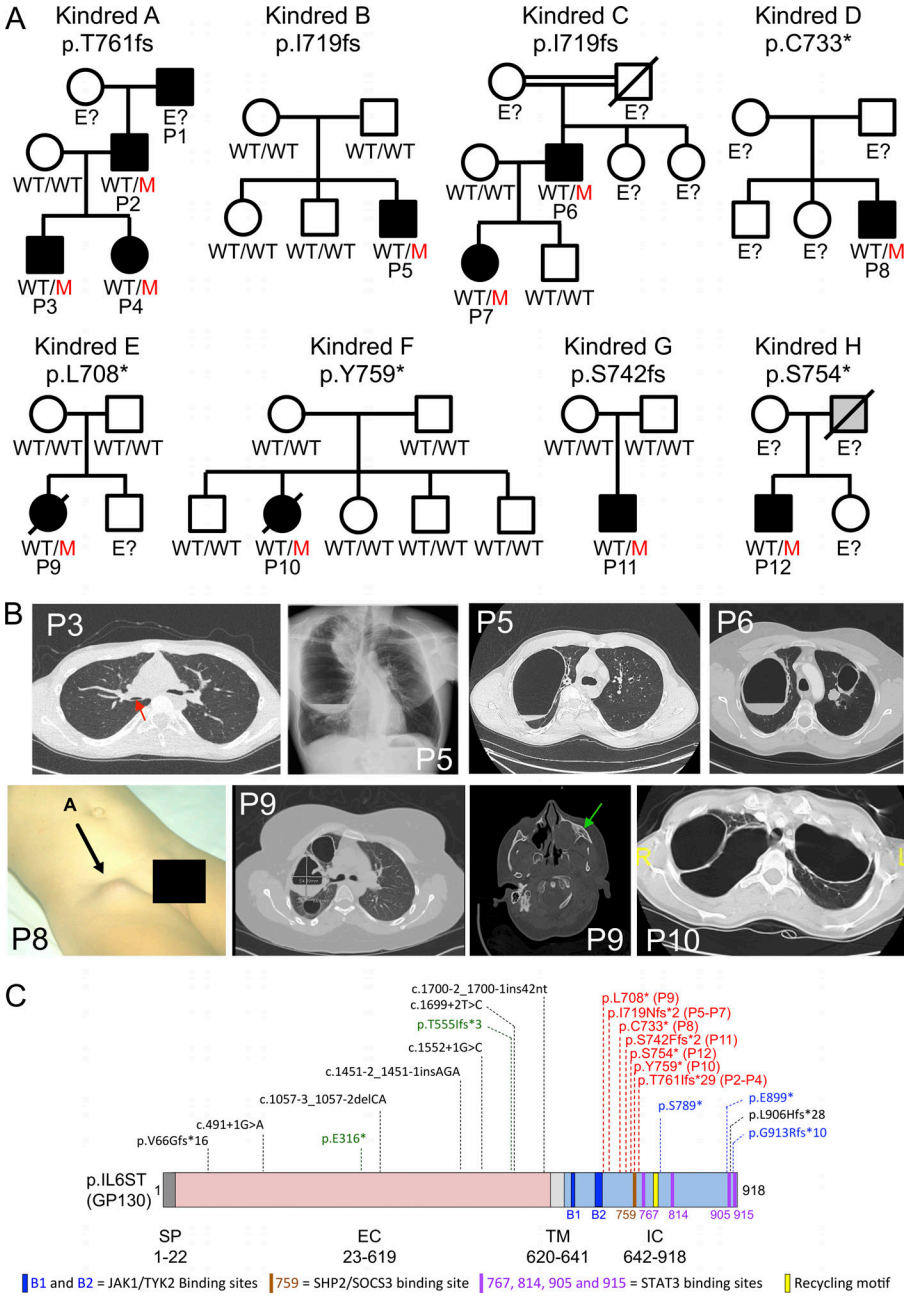


Figure 1. **AD IL6ST deficiency. (A)** Pedigree of the eight unrelated families showing familial segregation of the c.2277_2281dup (p.T761fs) mutant *IL6ST* allele in kindred A, the c.2155dup (p.I719fs) mutant *IL6ST* allele in kindreds B and C, the c.2199C>A (p.C733*) mutant *IL6ST* allele in kindred D, the c.2121del (p.L708*) mutant *IL6ST* allele in kindred E, the c.2277T>G (p.Y759*) mutant *IL6ST* allele in kindred F, the c.2224dup (p.S742fs) mutant *IL6ST* allele in kindred G, and the c.2261C>A (p.S754*) mutant *IL6ST* allele in kindred H. M, mutant. Individuals of unknown genotype are labeled "E?". The father of P12, who died at 26 yr of age, is shown in gray because he suffered from a phenotype partially compatible with HIES (asthma, multiple infections, rheumatoid arthritis, and diverticulitis). **(B)** Representative photographs and scanner images of patients, with scoliosis (P5), lung pneumatocele (P5, P6, P9, and P10), bronchomalacia (P3, red arrow), cold abscess (P8, black arrow), and sinusitis (P9, green arrow). **(C)** Schematic representation of GP130 and population genetics of *IL6ST* alleles. All reported predicted heterozygous "LOF" alleles and their positions in GP130 are indicated. The L708*, I719fs, C733*, S742fs, S754*, Y759*, and T761fs mutations found in the patients under study are colored in red. Mutants reported in gnomAD are colored in black, green, or blue. Two variants from gnomAD with a premature stop codon before the transmembrane domain were selected for subsequent functional analysis and are colored in green (E316* and T555fs). Three variants from gnomAD with a premature stop codon lacking one (G913fs), two (E899*), or three (S789*) STAT3-binding residues were selected for subsequent functional analysis and are colored in blue. EC, extracellular domain; IC, intracellular domain; SP, signal peptide; TM, transmembrane domain.

surface expression but with no STAT3 docking sites have been shown to exert a DN effect on IL-6 signaling (Kumanogoh et al., 1997; Selander et al., 2004).

### Population genetics of human *IL6ST*

Intriguingly, 13 predicted LOF heterozygous mutations in *IL6ST* (essential splicing site mutations, premature stop codons, and frameshift mutations), all with combined annotation-dependent depletion scores >20 and minor allele frequencies $<10^{-4}$, have been reported for 14 donors in the gnomAD database (Fig. 1 C; Zhang et al., 2018a). Nine of these reported rare variants are predicted to lack the transmembrane domain and, therefore, to abolish cell surface expression, suggesting that haploinsufficiency at the *IL6ST* locus is unlikely to be disease causing in our HIES patients. By contrast, the remaining four public LOF variants are predicted to be normally expressed at the cell surface and retain the STQPLL recycling motif (Dittrich et al., 1996). Moreover, these four variants lack only one (p.L906Hfs*28 and p.G913Rfs*10, hereafter referred to as G913fs), two (p.E899*), or three (p.S789*) of the four STAT3-binding residues (tyrosine 767, 814, 905, and 915) of GP130 (Fig. 1 C; Stahl et al., 1995). The p.L708*, p.I719fs, p.C733*, p.S742fs, p.S754*, p.Y759*, and p.T761fs mutations found in the eight HIES kindreds are, therefore, the only seven variants predicted to reach the cell surface and lack both the recycling motif and all four STAT3-binding sites within the IL6ST intracellular domain. The absence of all four STAT3-binding sites suggests that all seven mutations are LOF, and the lack of the recycling motif suggests that they accumulate at the cell surface, thereby potentially interfering with normal GP130 signaling via a DN mechanism. By contrast, the mutants reported

in gnomAD v2.1 are predicted to be LOF (but not DN, as they are not expressed at the cell surface), hypomorphic, or even isomorphic rather than DN, because they retain at least one STAT3-binding motif and are not overexpressed at the cell surface. Thus, the population genetics of *IL6ST* highlights the striking features specific to the variants seen in HIES patients.

### The HIES-associated GP130 mutants accumulate at the cell surface

Using CRISPR/Cas9, we first generated a human embryonic kidney (HEK) 293T cell line lacking GP130 expression (referred to hereafter as HEK-GP130-KO). We transfected HEK-GP130-KO cells with complementary DNAs (cDNAs) encoding WT GP130, two mutants lacking the transmembrane domain (E316* and T555fs), or mutants retaining the transmembrane domain but lacking one (G913fs), two (E899*), three (S789*), or four (L708*, I719fs, C733*, S742fs, S754*, Y759*, and T761fs) STAT3-binding residues (Fig. 1 C). SDS-PAGE of cell extracts followed by Western blotting and immunodetection with a monoclonal anti-GP130 antibody (clone E8, raised against amino acids 365–619) showed that the WT protein was produced at a mol wt of ∼140 kD, which is higher than the predicted mol wt (∼103 kD; Fig. 2 A). The T555fs (predicted mol wt ∼63 kD), L708* (predicted mol wt ∼80 kD), I719fs (predicted mol wt ∼82 kD), C733* (predicted mol wt ∼83 kD), S742fs (predicted mol wt ∼84 kD), S754* (predicted mol wt ∼85 kD), Y759* (predicted mol wt ∼86 kD), T761fs (predicted mol wt ∼89 kD), S789* (predicted mol wt ∼89 kD), E899* (predicted mol wt ∼101 kD), and G913fs (predicted mol wt ∼104 kD) mutants encoded truncated proteins with a mol wt above the predicted value (Fig. 2 A and Fig. S1 A). Surprisingly, the G913fs protein had a lower mol wt than the WT and E899* mutant proteins (Fig. 2 A). The extracellular domain of GP130 is highly N-glycosylated (Waetzig et al., 2010). We therefore investigated whether the observed differences with respect to the predicted mol wt were due to glycosylation and whether the G913fs mutation led to the production of an abnormally glycosylated protein. We treated cell protein extracts with peptide-N-glycosidase F (PNGase F) before SDS-PAGE and Western blotting. This resulted in the WT and all tested mutants migrating at a mol wt close to the expected value, confirming that the G913fs mutant was aberrantly N-glycosylated (Fig. 2 A). As expected, the E316* mutant (predicted mol wt ∼36 kD), which lacks the E8 mAb epitope, was not detected in either the presence or absence of PNGase F treatment. Extracellular staining and flow cytometry detected the WT and all the mutants except for E316* and T555fs, demonstrating that these two mutants lacking the transmembrane domain were not expressed at the cell surface (Fig. 2, B and C; and Fig. S1, B and C). The L708*, I719fs, C733*, S742fs, S754*, Y759*, and T761fs mutants, which lack the recycling motif, were all expressed about three to five times more strongly than the WT allele (Fig. 2, B and C; and Fig. S1, B and C). By contrast, the three truncated mutants retaining the recycling motif were normally (S789* and E899*) or less strongly (G913fs) expressed than the WT (Fig. 2, B and C). The low level of G913fs expression is accounted for by the aberrant glycosylation, as GP130 stability is dependent on glycosylation (Waetzig et al., 2010). These data suggest that all the mutants retaining the transmembrane domain are expressed at the cell surface, with higher levels of expression for the L708*, I719fs, C733*, S742fs, S754*, Y759*, and T761fs mutants, due to their accumulation at the cell surface in the absence of the recycling motif.

### The HIES-associated GP130 mutants are functionally deleterious

We then assessed STAT3 (Y705) and STAT1 (Y701) phosphorylation by flow cytometry in HEK-GP130-KO cells transfected with WT or mutant *IL6ST* cDNAs after stimulation with a chimeric IL-6/IL-6Rα protein (trans-signaling), which efficiently triggered GP130 signaling independently of other cytokine receptor subunits. Transfection with WT GP130 restored STAT3 and STAT1 phosphorylation in HEK-GP130-KO cells (Fig. 2 D). As expected, due to the lack of cell surface expression, transfection with E316* and T555fs failed to restore STAT1 and STAT3 phosphorylation (Fig. 2 D). Despite cell surface expression, transfection with the L708*, I719fs, C733*, S742fs, S754*, Y759*, and T761fs mutants, lacking all four STAT3-binding sites, completely failed to restore STAT3 phosphorylation, whereas weak STAT1 phosphorylation was detected (Fig. 2 D and Fig. S1, D and E). By contrast, mutants retaining the transmembrane domain but lacking only one (G913fs), two (E899*), or three (S789*) STAT3-binding sites retained the ability to phosphorylate both STAT1 and STAT3. Phosphorylation levels were, nevertheless, very low for G913fs, possibly due to its abnormal N-glycosylation and weaker expression (Fig. 2, A–D; Waetzig et al., 2010). By contrast, HEK-GP130-KO cells transfected with any of the GP130 variants displayed normal STAT1 and STAT3 phosphorylation in response to stimulation with IFN-α (Fig. 2 D and Fig. S1, D and E). Using the same system, but with IL-6 or IL-11 stimulation, we found that only the WT allele could restore low levels of STAT3 phosphorylation (Fig. S1 D). Transfection with GP130 mutants from HIES patients restored low levels of STAT1 phosphorylation after IL-27 stimulation and of STAT3 phosphorylation after stimulation with LIF or OSM (Fig. S1, D and E), possibly due to the intrinsic signaling potential of IL-27RA, LIF-R, and OSM-R (Nicola and Babon, 2015; Hermanns, 2015; Murakami et al., 2019). We then used a reporter assay to assess the ability of each mutant to activate STAT3 signaling (Fig. 2 E and Fig. S2, A and B). We cotransfected HEK-GP130-KO cells with an empty vector (EV), plasmids encoding the WT or mutant GP130 proteins, and a plasmid containing a luciferase reporter gene under the control of five SIS-inducible elements (SIEs). IFN-α stimulation was used as a positive control and induced luciferase in all transfection conditions tested (Fig. S2 B). WT *IL6ST* transfection induced strong luciferase activity upon stimulation with each of the GP130-dependent cytokines tested: IL-6, IL-6/IL-6Rα, IL-11, IL-27, LIF, and OSM (Fig. 2 E and Fig. S2 A). As reported for transfection with the EV, transfection with the E316* or T555fs mutants led to no induction of luciferase activity upon stimulation with any of the GP130-dependent cytokines, confirming that these two mutants were completely LOF. Mutants lacking one to three STAT3-binding sites (S789*, E899*, and G913fs) consistently failed to respond to IL-6 and IL-11 but had normal or

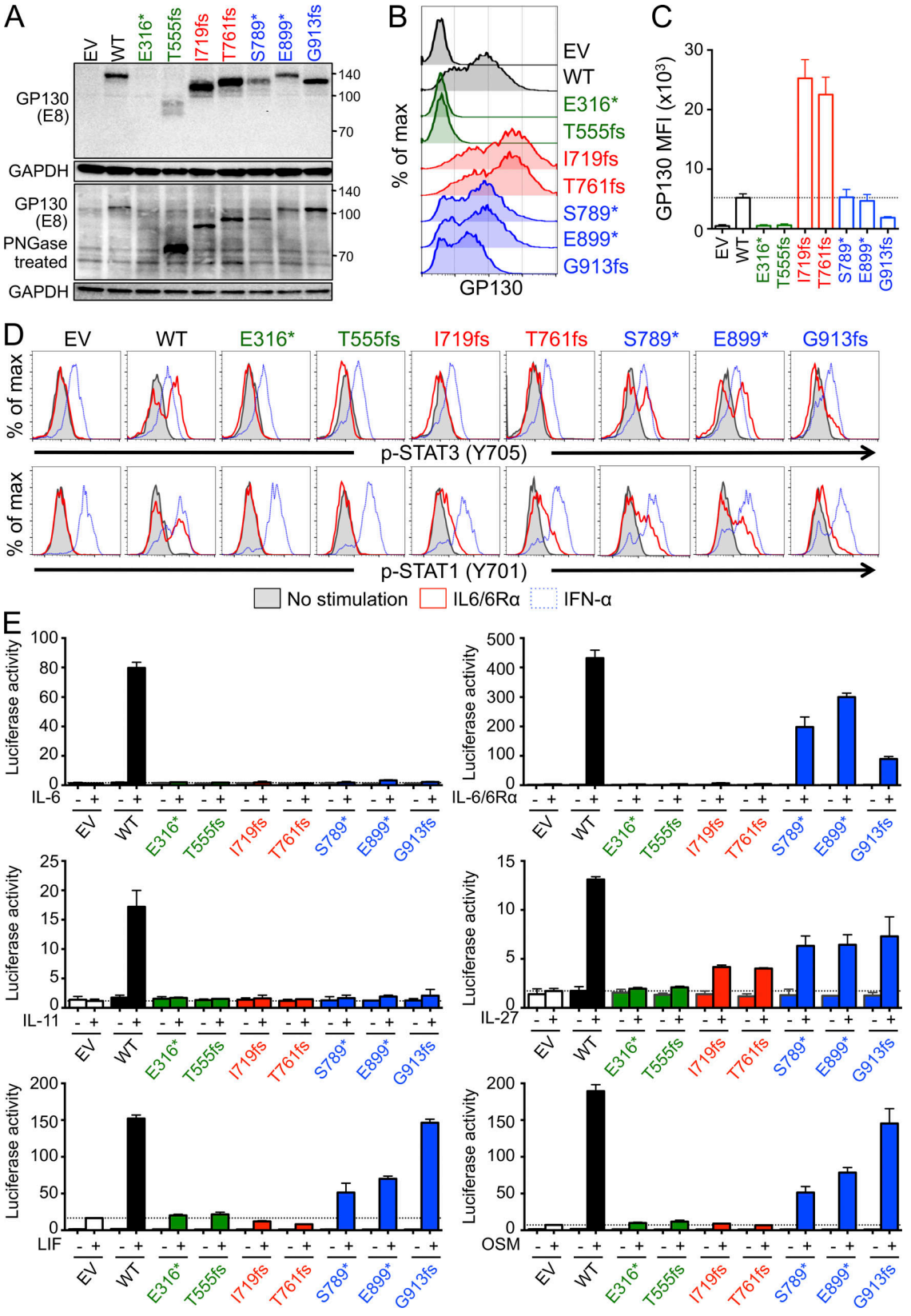


Figure 2. **The I719fs and T761fs *IL6ST* mutants accumulate at the cell surface and are LOF. (A)** GP130-deficient HEK293T cells were transfected with an empty pCMV6 plasmid (EV) or with pCMV6 plasmids encoding the WT or the E316*, T555fs, I719fs, T761fs, S789*, E899*, or G913fs GP130 mutants. Total protein was extracted, left untreated (top), or treated (bottom) for 1 h with PNGase F to eliminate N-glycosylation, and subjected to immunoblotting with a mAb against GP130 (amino acids 365–619, clone E8). GAPDH was used as a loading control. Western blots representative of three independent experiments are shown. **(B and C)** GP130-deficient HEK293T cells were transfected as described in A. After 48 h of incubation, cells were harvested, stained for extracellular

GP130 expression, and analyzed by flow cytometry. An image showing representative staining (B) and a recapitulative graph depicting GP130 mean fluorescence intensity (MFI; C) are shown. The bars and error bars represent the mean of three different experiments and the standard deviation, respectively. **(D)** GP130-deficient HEK293T cells were transfected as described in A. After 24 h of incubation, the cells were stimulated for 15 min with IL-6/IL-6Rα or IFN-α, or left unstimulated, and the phosphorylation of STAT1 (pY701) and of STAT3 (pY705) was then evaluated. Representative results from three independent experiments are shown. **(E)** Luciferase assay to assess STAT3 activity. GP130-deficient HEK293T cells were transfected with an empty pCMV6 vector (EV) or a plasmid encoding the WT or the indicated GP130 mutants, plus a pGL4.47 reporter plasmid carrying the luciferase cDNA downstream from five SIEs. After 24 h, cells were stimulated with the indicated cytokine (+) or were left unstimulated (–) for another 24 h before the measurement of luciferase activity. The horizontal dotted line indicates the luciferase activity after stimulation, with the indicated cytokine, of the cells transfected with the empty pCMV6 vector. The results shown are the mean and standard error of the mean for a technical duplicate. Luciferase assays representative of three independent experiments are shown.

only partially impaired responses to IL-6/IL-6Rα, IL-27, LIF, and OSM. By contrast, mutants lacking all four STAT3-binding sites (L708*, I719fs, C733*, S742fs, S754*, Y759*, and T761fs) were LOF for all cytokines tested, except for IL-27, for which the response was weak (approximately one third of WT levels), but not abolished. This partial response to IL-27 could be explained by intrinsic signaling capacity of the intracellular domain of IL-27RA (Pflanz et al., 2004). The T761fs mutant from P2 to P4 was the only variant retaining the tyrosine in position 759 of GP130 (Y759) previously shown to recruit SHP2 and activate the MAPK pathway (Stahl et al., 1995; Symes et al., 1997; Schaper et al., 1998; Kim et al., 1998). An erythropoietin receptor–GP130 fusion protein (extracellular domain of erythropoietin receptor fused to the intracellular domain of GP130) including a GP130 intracellular tail lacking all four STAT3-binding sites but retaining Y759 has been reported to activate the MAPK pathway in response to Epo despite impaired STAT3 activation (Lehmann et al., 2003). We therefore assessed ERK1/2 phosphorylation in the MAPK pathway by flow cytometry in HEK-GP130-KO cells transfected with WT or selected mutant *IL6ST* cDNAs, after stimulation with a chimeric IL-6/IL-6Rα protein (Fig. S2 C). We confirmed that the WT allele induced the phosphorylation of ERK1/2 and that the T761fs mutant retained a weak but consistent ability to induce ERK1/2 phosphorylation, whereas the other two mutants tested, I719fs and S754*, did not. Overall, these data suggest that when overexpressed in isolation, the L708*, I719fs, C733*, S742fs, S754*, Y759*, and T761fs mutants are the only mutants retaining surface expression that are completely LOF for STAT3 activation for all GP130-dependent cytokines tested, with the exception of IL-27, for which the response was weak, but not abolished. T761fs was the only mutant tested that retained the ability to activate the MAPK pathway due to its retention of the SHP2-recruiting motif.

### The HIES-associated GP130 mutants are DN

As suggested by the population genetics analysis, there seems to be no haploinsufficiency at the human *IL6ST* locus (Fig. 1 C). We therefore tested the hypothesis that the L708*, I719fs, C733*, S742fs, S754*, Y759*, and T761fs mutants exert a DN effect on the WT allele. Using the luciferase system described above, we assessed the impact of increasing the concentrations of the plasmids encoding various mutant alleles of *IL6ST* cDNA while keeping the concentration of the plasmid encoding the WT *IL6ST* cDNA constant (Fig. 3 and Fig. S3, A–G). IFN-α stimulation was used as a positive control and induced luciferase in all transfection conditions tested (Fig. 3 and Fig. S3 G). Mutants lacking the transmembrane domain (E316* and T555fs) or only one STAT3-binding site (G913fs) had no DN effect on WT GP130 at any mutant:WT (Mut:WT) concentration ratio, following stimulation with any of the six cytokines (IL-6, IL-11, IL-6/IL-6Rα, IL-27, LIF, and OSM; Fig. S3, A–F). As expected, mutants lacking all four STAT3-binding sites (L708*, I719fs, C733*, S742fs, S754*, Y759*, and T761fs) exerted a potent DN effect for all cytokines tested (Fig. 3 and Fig. S3, A–F). This DN effect was very strong at low Mut:WT ratios (0.5:1 and 1:1) for IL-6 and IL-11 signaling but was effective at higher Mut:WT ratios (4:1 and 8:1) for the other cytokines tested (IL-6/IL-6Rα, IL-27, LIF, and OSM). The DN effect on IL-27 and IL-6/IL-6Rα signaling was incomplete, even at the highest Mut:WT ratio tested. Mutants lacking two (E899*) or three (S789*) STAT3-binding sites were not DN following IL-6/IL-6Rα stimulation for any of the Mut:WT ratios tested (Fig. S3 B). They had little impact on IL-27, LIF, and OSM signaling, even at high Mut:WT ratios. However, they exerted a potent DN effect on IL-6 and IL-11 signaling, although this effect was weaker than that observed with the I719fs and T761fs mutants (Fig. S3, A and C). Given the stronger DN effect of the HIES-causing mutants on IL-6 signaling than IL-6/IL-6Rα trans-signaling, which does not require membrane-anchored IL-6Rα expression on target cells, we hypothesized that a limited pool of IL-6R might accentuate the DN effect of the mutants on IL-6 signaling. We tested this hypothesis with the luciferase system described above by cotransfecting HEK-GP130-KO cells with *IL6R* WT cDNA together with WT GP130 alone, I719fs GP130 alone, or WT plus I719fs GP130 (ratio 1:1) before IL-6 stimulation (Fig. 4). IL-6/IL-6Rα stimulation (trans-signaling) was performed in parallel for comparison. At a 1:1 Mut:WT ratio, as shown in our previous experiment (Fig. 3), the I719fs mutant exerted a potent DN effect on IL-6 signaling, but not on IL-6/IL-6Rα trans-signaling. By contrast, in the same experimental conditions, cotransfection with IL-6R abolished the DN effect of the I719fs mutant (Fig. 4). Overall, these data show that L708*, I719fs, C733*, S742fs, S754*, Y759*, and T761fs mutants, the only mutants identified that accumulate at the cell surface, exert a strong DN effect for all GP130-dependent cytokines tested, including IL-6 trans-signaling (IL-6/IL-6Rα). The DN effect on "classic" IL-6 signaling exerted by the various *IL6ST* mutants was due, at least in part, to the hijacking of the limited pool of transmembrane IL-6R, accounting for the smaller impact on IL-6 trans-signaling.

### GP130 production and function in primary fibroblasts from patients

Given the skeletal abnormalities observed in the DN GP130 patients, we used flow cytometry to assess GP130 in primary

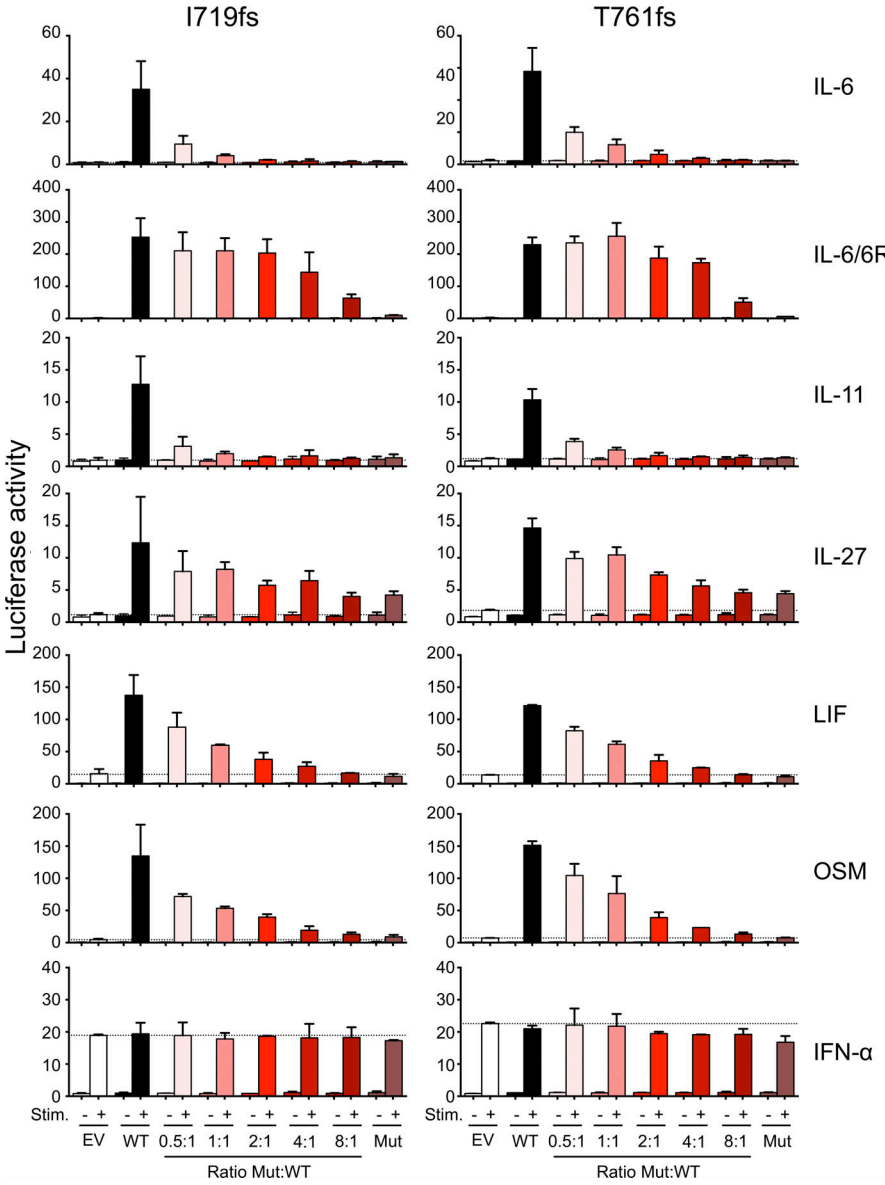


Figure 3. **The I719fs and T761fs GP130 mutants are DN over the WT GP130.** GP130-deficient HEK293T cells transfected with a pCMV6 EV or encoding the WT GP130 (25 ng) and various concentrations (25–200 ng) of pCMV6 vector encoding the indicated GP130 mutants (Mut) plus a pGL4.47 reporter plasmid carrying the luciferase cDNA downstream from five SIEs. GP130-deficient HEK293T cells transfected with only the WT (25 ng) or the mutant GP130 (200 ng) were used as controls. Cells were stimulated, 24 h after transfection, with the indicated cytokine (+) or were left unstimulated (–) for another 24 h before the measurement of luciferase activity. The results shown are the mean and standard error of the mean for a technical duplicate. Luciferase assays representative of two independent experiments are shown.

fibroblasts from patients and healthy controls (Fig. 5, A and B). We found that the fluorescence intensity of GP130 in P2 (T761fs) and P5 (I719fs) was approximately seven times higher than that in healthy controls. Western blotting suggested that these higher levels of surface GP130 expression on flow cytometry were due to the accumulation of the mutant proteins at the cell surface (Fig. 5 C). Indeed, we detected normal levels of the WT protein and abnormally large amounts of the truncated mutant proteins in the fibroblasts of P2 and P5. Relative quantification of the bands showed that the T761fs (~89 kD) and I719fs (~82 kD) mutant proteins were approximately five and seven times more abundant than the WT protein in P2 and P5, respectively. Primary fibroblasts from P6 and P7 were then cultured for 30 min to 4 h in the presence of cycloheximide (to block de novo protein synthesis) before flow cytometry to assess GP130 expression (Fig. S4 A). GP130 cell surface expression was more stable in the fibroblasts of the patients than in those of the controls, suggesting a slower rate of degradation, consistent with the absence of the recycling motif in the mutant proteins. We therefore assessed STAT1 and STAT3 phosphorylation in primary fibroblasts from P2, P5, and P9 after starvation in the absence of serum, comparing the results obtained with those for controls. IL-6/IL-6Rα and OSM induced strong STAT1 and STAT3 phosphorylation in the cells of both controls and patients (Fig. 5 D). LIF induced the phosphorylation of STAT3 only in both controls and patients. IL-6 stimulation induced STAT3 phosphorylation in the controls, but not in P2, P5, and P9 (Fig. 5 D and Fig. S4 B). By contrast, IL-11 stimulation induced STAT3 phosphorylation in the controls and P2, but not in P5 and P9. No STAT1 phosphorylation in response to IL-11 stimulation was detected in the controls or the patients. Thus, due to mutant GP130 accumulation at the cell surface, STAT3 phosphorylation in response to IL-11 stimulation is strongly impaired in the fibroblasts from P5 and P9, consistent with the marked skull phenotype of these patients. The normal response of P2 fibroblasts to IL-11 stimulation is consistent with the milder skeletal abnormalities observed in kindred A. The

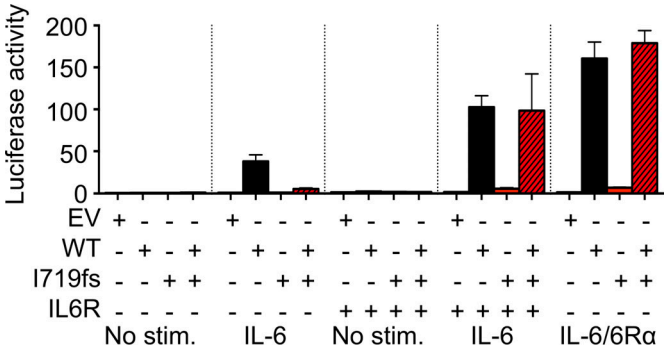


Figure 4. **DN mutants hijack IL-6R.** GP130-deficient HEK293T cells transfected with an empty pCMV6 vector or a vector encoding the WT GP130 (25 ng) and a pCMV6 vector encoding the I719fs GP130 mutant (25 ng) plus a pGL4.47 reporter plasmid carrying the luciferase cDNA downstream from five SIEs. GP130-deficient HEK293T cells transfected with only the WT (25 ng) or the mutant GP130 (25 ng) were used as controls. A pCMV6 vector encoding IL-6R (25 ng) was also used for cotransfection, where indicated. Cells were stimulated with IL-6 or IL-6 plus IL-6Rα, as indicated, 24 h after transfection or were left unstimulated for another 24 h before the measurement of luciferase activity. The results shown are the mean and standard error of the mean for a technical duplicate. Luciferase assays representative of two independent experiments are shown.

variability of IL-11 responses observed in vitro in fibroblasts carrying slightly different *IL6ST* mutations remains unexplained. Subtle differences in functional properties between the mutants (e.g., the ability to activate the MAPK pathway) may contribute to these clinical differences. The impairment of these responses appears to be correlated with the severity of the HIES phenotype observed in patients bearing DN mutations of *IL6ST*.

### *IL6ST* mutations underlie typical immunological phenotypes of HIES

Before investigating the production and function of GP130 in leukocyte subsets, we analyzed the development of these subsets in patients. The patients' inflammatory responses were not abolished, at odds with the IL6ST-AR and IL6R-AR deficiencies (Schwerd et al., 2017; Spencer et al., 2019), as illustrated by the fever and increase in C-reactive protein (CRP) levels observed during infection, at least in P5, P6, and P10 (Fig. 6). Leukocyte counts were normal in all patients except P3, who had low leukocyte counts. Within the myeloid compartment, neutrophils and monocytes were present, and, overall, their numbers were within the normal range (Table S2). Monocyte subsets and dendritic cell subsets were present in normal proportions among monocytes and peripheral blood mononuclear cells (PBMCs), respectively (Fig. 7, A and B). Eosinophil counts were high in P5, P6, P7, P9, and P10 (Table S2). Lymphocyte counts were normal in all patients except P2, who repeatedly had low counts (Table S2). Within the lymphoid compartment, B cell counts were normal in all patients except P8, who had low counts, and P11 and P12, who had elevated counts (Table S2). The frequency of $CD27^+$ memory B cells was low in all tested patients (Fig. 7 C). Among memory B cells, the frequencies of $IgM^+$ and $IgG^+$ cells were normal, whereas the frequency of $IgA^+$ was slightly but significantly lower than normal (Fig. 7 D). Consistent with these findings, serum concentrations of IgG and IgG subclasses were normal, except in P2 and P6, who had low levels of total IgG and IgG subclasses (Table S2). Serum IgE concentration was high in all patients (Table S2). The patients had normal serum titers of antigen-specific antibodies after infection with common pathogens, except for P6, who lacked varicella zoster virus–specific IgG despite a reported history of chickenpox (Table S3). Low-to-normal levels of IgG against *Haemophilus influenzae*, diphtheria, and tetanus vaccines were detected in all vaccinated patients (Table S3). Natural killer (NK) cell counts and differentiation were normal in all patients, except P6 and P9, who had low NK cell counts (Fig. 7, E–G; and Table S2). $CD4^+$ and $CD8^+$ T cell counts were normal except in P2 and P11, who had low $CD8^+$ T cell counts and high $CD4^+$ T cell counts, respectively (Table S2). Within the $CD4^+$ and $CD8^+$ T cell compartments, patients had high naive and low central memory T cell frequencies, respectively (Fig. 7, H and I). The patients' $CD8^+$ T cells also contained a low proportion of effector memory T cells (Fig. 7 I). The proportions of γδ T cells, invariant natural killer T (iNKT) cells, and regulatory T (T reg) cells were normal, and the proportion of mucosal-associated invariant T (MAIT) cells was low (Fig. 7, J and K). Within the memory $CD4^+$ T cell compartment, the frequency of T follicular helper (Tfh) cells was low, whereas the frequencies of T helper type 1 (Th1), Th17, and Th1* cells were normal and those of Th2 cells were very high (Fig. 7 L). This distribution of leukocyte subsets bears some resemblance to that of patients with AD-HIES due to *STAT3* DN mutations, who have high frequencies of naive $CD4^+$ T cells, low frequencies of central memory $CD4^+$ and $CD8^+$ T cells, MAIT cells, and memory B cells, and high proportions of Th2 cells and low proportions of Th1* and Th17 cells within the memory $CD4^+$ T cell compartment (Avery et al., 2010; Minegishi et al., 2007; Chandesris et al., 2012b; Ma et al., 2012, 2015; Siegel et al., 2011; Wilson et al., 2015). Overall, the immunological phenotypes of patients with *STAT3* and *IL6ST* mutations are similar, except for the normal Th17 and Th1* frequencies and detectable signs of the acute phase in patients with *IL6ST* DN mutations.

### *IL6ST* mutations induce a strong increase in Th2 cytokine production

For confirmation of the results of T helper cell immunophenotyping, we assessed the capacity of the patients' memory $CD4^+$ T cells to secrete Th1, Th2, and Th17 cytokines. We sorted $CD4^+$ memory T cells from three patients and 12 controls and cultured them for 5 d with beads coated with monoclonal antibodies against CD3, CD2, and CD28 and then performed cytokine determinations on the supernatant. The patients' memory $CD4^+$ T cells produced normal levels of IL-2 and Th1 cytokines (TNF and IFN-γ; Fig. 8 A). In contrast, all three Th2 cytokines examined (IL-4, IL-5, and IL-13) were strongly increased in culture supernatants of patient memory $CD4^+$ T cells compared with controls (Fig. 8 B). Th17 cytokine levels were significantly decreased for IL-17F and IL-22, but not IL-17A (Fig. 8 C). Moreover, the frequency of $IL\text{-}17A^+$, $IL\text{-}17F^+$, and $IL\text{-}22^+$ memory $CD4^+$ T cells after 5 d of culture with beads coated with mAbs against CD3, CD2, and CD28 was also significantly decreased (Fig. 8 D). Finally, we sorted naive $CD4^+$ T cells from DN *IL6ST* patients and healthy controls; cultured them with beads coated with mAbs against CD3, CD2, and CD28 in the presence or absence of a Th17-polarizing cytokine mixture; and measured Th17 cytokine

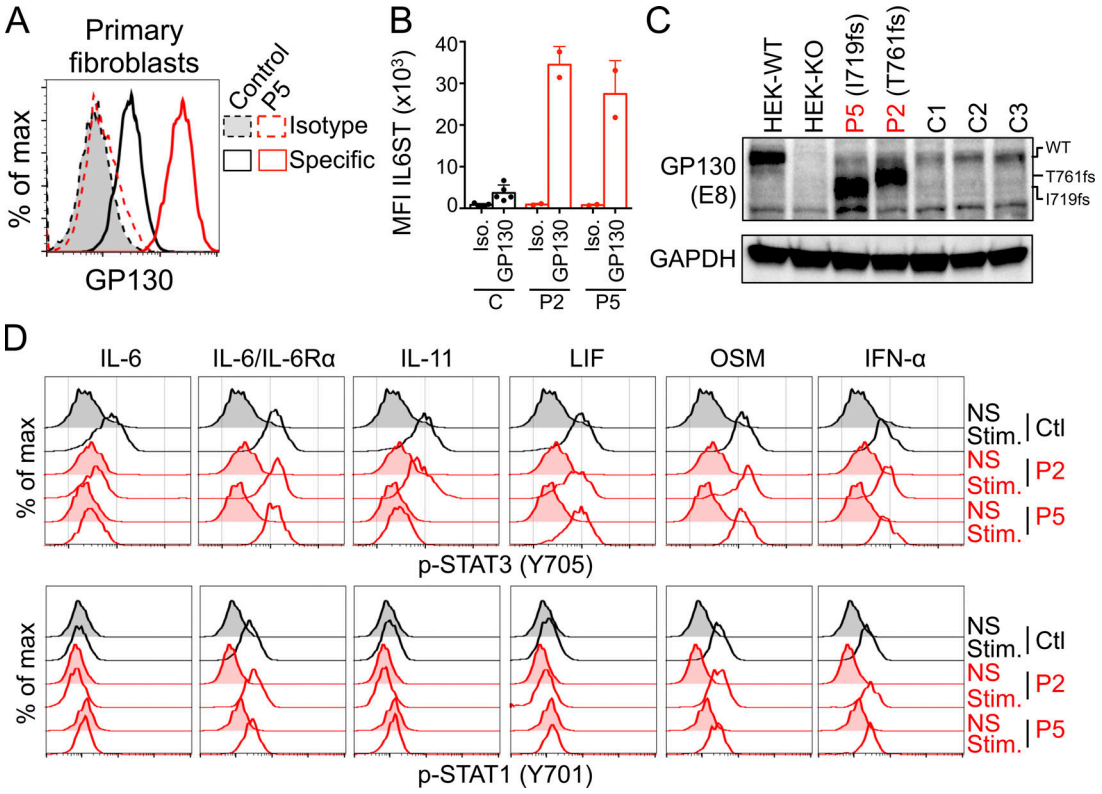


Figure 5. **GP130 production and activity in the patients' primary fibroblasts. (A and B)** GP130 levels in primary fibroblasts, as evaluated by flow cytometry. **(A)** Representative traces of GP130 expression in primary fibroblasts from P5 and a healthy control are shown, together with traces for the isotypic control. **(B)** The graph shows the MFI of GP130 in five independent controls, and two patients (P2 and P5). The bars and error bars for the patients represent the mean of a duplicate and the standard deviation, respectively. **(C)** Total protein was extracted from primary fibroblasts and subjected to immunoblotting with a mAb against GP130 (amino acids 365–619, clone E8). GAPDH was used as a loading control. Western blots representative of three independent experiments are shown. **(D)** Primary fibroblasts from P2 and P5 and three healthy controls (Ctl, only one shown) were stimulated (Stim) for 15 min with IL-6, IL-6/IL-6Rα, IL-11, LIF, OSM, and IFN-α or left unstimulated (NS), and the phosphorylation of STAT3 (pY705, top panel) and STAT1 (pY701, bottom panel) was then evaluated by flow cytometry. FACS plots representative of two independent experiments are shown.

secretion after 5 d of stimulation. Patients' and controls' naive CD4⁺ T cells secreted similar levels of IL-17A and IL-17F (Fig. 8 E). Taken together, these in vitro data reveal an increased Th2 cell response and a modestly impaired Th17 cell response in DN *IL6ST* patients compared with normal controls. The strong Th2 cell response may account for the high IgE levels and allergies in the patients, whereas the apparently subnormal Th17 cell response is consistent with the rarity of CMC, which was observed in only 1 of the 12 patients.

### *IL6ST* expression is up-regulated in the patients' PBMCs

We used flow cytometry to assess GP130 expression in PBMC subsets from six patients (P2–P7) and controls in basal conditions (Fig. 9, A–E). We detected no GP130 expression in the CD56$^{dim}$ and CD56$^{bright}$ NK cells of controls and patients (Fig. 9 A). GP130 expression was also undetectable in naive and memory B cells from the controls, whereas weak GP130 expression was detectable in naive and memory B cells from the patients (Fig. 9 B). GP130 expression was detectable in control and P8-derived EBV-B cell lines, and, as in primary B cells, GP130 levels were higher in the patients' cells than in control cells (Fig. S5 A). GP130 was expressed strongly in the naive CD4⁺ and CD8⁺ T cells, and to a lesser extent in memory CD4⁺ T cells, from both controls and patients (Fig. 9, C and D). GP130 levels were slightly but significantly higher in the CD4⁺ and CD8⁺ naive T cells of patients (P2–P7) than in those of controls (Fig. 9, C and D). No GP130 expression was detected in the CD8⁺ memory

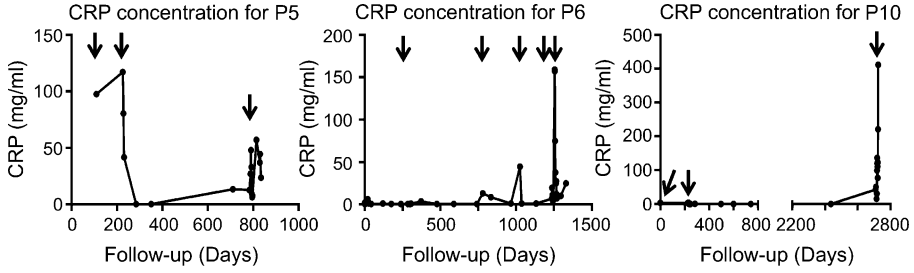


Figure 6. **Serum CRP levels suggest normal acute phase in patients.** CRP kinetics of P5, P6, and P10, and CRP levels in P5, P6, and P10 during the follow-up period. Arrows indicate infections.

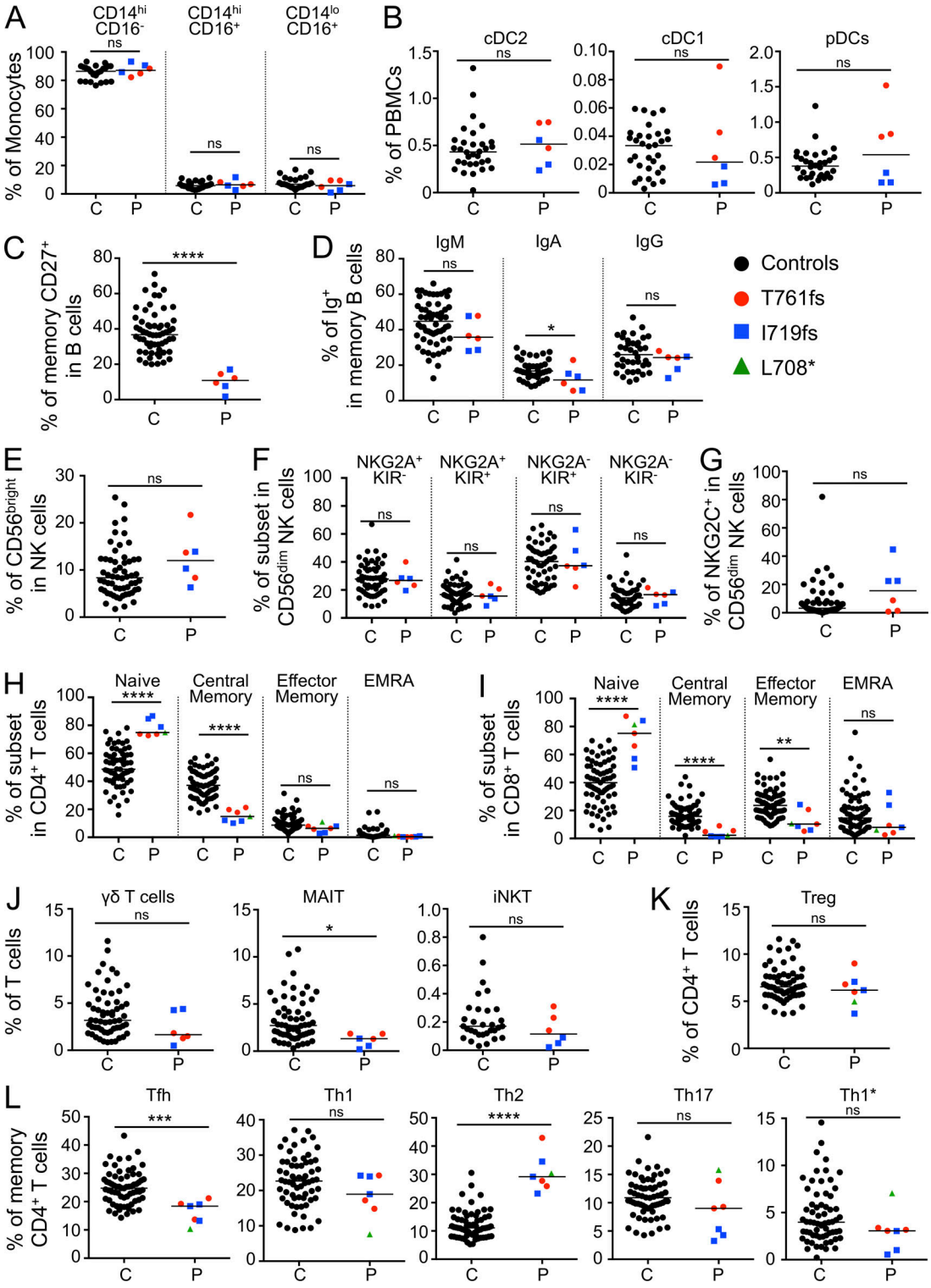


Figure 7. **Leukocyte immunophenotyping. (A)** Frequencies of monocyte subsets, as assessed by measuring the expression of CD16 and CD14, for controls ($n$ = 23; C) and patients (P) with AD *IL6ST* mutations ($n$ = 6). ns, not significant. **(B)** Frequencies of cDC2 (Lin$^-$HLA-DR$^+$CD11c$^+$CD1c$^+$CD141$^-$), cDC1 (Lin$^-$HLA-DR$^+$CD11c$^+$CD1c$^-$CD141$^+$), and plasmacytoid DCs (Lin$^-$HLA-DR$^+$CD11c$^-$CD123$^+$) among the PBMCs of controls ($n$ = 32) and patients with AD *IL6ST* mutations ($n$ = 6). **(C)** Frequency of CD27$^+$ memory cells within the B cell compartment of controls ($n$ = 60) and patients with AD *IL6ST* mutations ($n$ = 6). **(D)** Frequency of IgM$^+$, IgA$^+$, and IgG$^+$ cells within the memory B cell compartment of controls ($n$ = 39–60) and patients with AD *IL6ST* mutations ($n$ = 6). **(E–G)** NK cell immunophenotyping for controls ($n$ = 58–60) and patients with AD *IL6ST* mutations ($n$ = 6), showing the frequency of CD56$^{bright}$ cells within the NK-cell compartment (E), the terminal differentiation profile of the CD56$^{dim}$ compartment (F), and the frequency of NKG2C$^+$NKG2A$^-$ cells within the CD56$^{dim}$ compartment (G). **(H and I)** Frequency of naive (CD45RA$^+$CCR7$^+$), central memory (CD45RA$^-$CCR7$^+$), effector memory (CD45RA$^-$CCR7$^-$), and $T_{EMRA}$ (CD45RA$^+$CCR7$^-$) cells among the CD4$^+$ (H) and CD8$^+$ (I) T cells of controls ($n$ = 65) and patients with AD *IL6ST* mutations ($n$ = 7). **(J)** Frequency of γδ T cells

(CD3⁺TCR-γδ⁺), MAIT (CD3⁺CD161⁺TCR-vα7.2⁺), and iNKT (CD3⁺TCR-iNKT⁺) cells among the T cells of controls ($n$ = 31–59) and patients with AD *IL6ST* mutations ($n$ = 6). **(K)** Frequency of T reg (CD3⁺CD4⁺CD25$^{hi}$FoxP3⁺) cells in the CD4⁺ T cell compartment of controls ($n$ = 59) and patients with AD *IL6ST* mutations ($n$ = 7). **(L)** Frequency of Th subsets within the CD4⁺ memory compartments of controls ($n$ = 60–64), and patients with AD *IL6ST* mutations ($n$ = 7). Subsets were defined as follows: Tfh (CXCR5⁺), Th1 (CXCR5⁻CXCR3⁺CCR4⁻CCR6⁻), Th2 (CXCR5⁻CXCR3⁻CCR4⁺CCR6⁻), Th1* (CXCR5⁻CXCR3⁺CCR4⁻CCR6⁺), and Th17 (CXCR5⁻CXCR3⁻CCR4⁺CCR6⁺). **(A–L)** $t$ tests were used for all comparisons.

T cells of patients or controls (Fig. 9 C). GP130 levels in control PBMCs were high in monocytes, and the patients' monocytes had GP130 levels approximately three times higher than those in control monocytes (Fig. 9 E). We assessed the impact of DN mutations of *IL6ST* on lymphocyte subsets by assessing STAT1 and STAT3 phosphorylation in CD4⁺ and CD8⁺ T cells (P5–P7), and B cells from patients (P2–P7), in response to simulation with IL-6, IL-6/IL-6Rα, IL-27, or IFN-α (Fig. 9, F and G; and Fig. S5, B and C). STAT3 phosphorylation in CD4⁺ and CD8⁺ cells in response to IL-6, IL-6/IL-6Rα, and IL-27 was partially impaired relative to controls. STAT3 phosphorylation in response to IL-6/IL-6Rα and IL-27 was detected in control B cells, suggesting that they express some GP130 despite of its lack of detection by flow cytometry. STAT3 phosphorylation in response to IL-6/IL-6Rα or IL-27 was much weaker in the patients' B cells than in control B cells, consistent with the higher levels of GP130 detected only in the patients' cells. We also stimulated EBV-B cells from P8 with IL-6 and IL-27. These cells responded poorly to IL-6 but, unlike primary B cells, their response to IL-27 was normal and similar to that of controls (Fig. S5 D). We then sorted monocytes from P5 and assessed STAT1 and STAT3 phosphorylation after the stimulation of these cells with IL-6, IL-6/IL-6Rα, IL-27, or IFN-α (Fig. 9 G). STAT3 phosphorylation was almost totally abolished in the patients' monocytes in response to IL-6, IL-6/IL-6Rα, or IL-27. STAT1 phosphorylation in response to IL-27 stimulation was detected in lymphocytes and monocytes and was similar in controls and patients. No STAT1 phosphorylation was detected in response to IL-6 and IL-6/IL-6Rα in the lymphocytes and monocytes of controls or patients. All subsets from patients and controls responded to IFN-α, which served as a positive control. We also observed normal STAT3 phosphorylation after stimulation with IL-10 or IL-21 in B cells and EBV-B cells from the patients; both these cytokines are GP130 independent (Fig. S5, C and D). These data show that GP130 accumulation at the cell surface is cell-type dependent and that STAT3 phosphorylation in response to stimulation with GP130-dependent cytokines is impaired in the patients' lymphocytes and monocytes. The strong B cell defect observed ex vivo is consistent with the impaired B cell immunity of the patients in vivo.

## Discussion

We describe here a form of AD-HIES caused by DN *IL6ST* variants in 12 patients from 8 unrelated kindreds without *STAT3* mutations. The patients have a typical clinical presentation of AD-HIES with pulmonary infections, severe cystic bronchiectasis, eczema, abnormalities of bones and teeth, and high IgE levels but with apparently normal acute-phase responses. Impaired responses to IL-11 (and perhaps LIF) probably account for most of the skeletal abnormalities, whereas impaired responses to IL-6 probably account for most of the immunological abnormalities. However, unlike patients with AR partial GP130 or complete IL11RA deficiency, patients with AD GP130 deficiency do not have craniosynostosis, presumably due to residual responses to IL-11 via GP130 (Schwerd et al., 2017; Shahin et al., 2019; Nieminen et al., 2011). Patients with AD-GP130 deficiency lack the pathognomonic features of SWS (Mikelonis et al., 2014), reflecting the presence of residual LIF signaling. Similarly, CMC (P9) and skin abscesses (P6, P8, P10, and P12) were reported in only a few patients and thus at a frequency lower than that in HIES patients with *STAT3* mutations (Chandesris et al., 2012b). This observation is consistent with the near-normal counts of Th17 cells in the patients described here, at odds with the data for patients with *STAT3* mutations (Milner et al., 2008; Ma et al., 2008, 2015, 2016; de Beaucoudrey et al., 2008). Near-normal Th17 cell levels and a lack of CMC were observed in patients with biallelic null mutations of *IL6R*, *IL23R*, or *IL21R* (Kotlarz et al., 2013; Martínez-Barricarte et al., 2018; Spencer et al., 2019; Ma et al., 2016). This suggests that IL-6R, IL-21R, and IL-23R are individually, but not collectively, redundant for Th17 cell differentiation, accounting for CMC in patients with DN STAT3 or AR ZNF341 deficiency, whose cellular responses to IL-6, IL-21, and IL-23 are all impaired. AR complete GP130 deficiency causes a SWS-like disorder with perinatal mortality (Monies et al., 2019; Chen et al., 2020). Otherwise, the AR and AD forms of partial GP130 deficiency display a considerable overlap, except for the lack of craniosynostosis and apparently normal acute-phase response in the AD form. This suggests that the two different modes of inheritance of *IL6ST* defects affect overlapping cellular responses to cytokines of the IL-6 family. Other *IL6ST* genotypes may underlie various clinical phenotypes, depending on the nature of the mutation.

The relatively selective effect of mutant GP130 proteins lacking all four STAT3-binding sites on the different members of the IL-6 family of cytokines can be explained by the intrinsic signaling capacity of the coreceptors. IL-6 and IL-11 bind IL-6R and IL-11R, respectively, with high affinity, and they then recruit GP130 (Taga et al., 1989; Hibi et al., 1990; Yamasaki et al., 1988; Hilton et al., 1994; Chérel et al., 1995). By contrast, LIF-R, OSM-R, and IL-27RA have a low affinity for their respective ligands, and they require GP130 to form high-affinity receptors (Gearing et al., 1992; Pflanz et al., 2004). Moreover, IL-6R and IL-11R chains have short intracellular tails and are therefore strictly dependent on GP130 for STAT3 activation (Yamasaki et al., 1988; Hilton et al., 1994). By contrast, LIF-R, OSM-R, and IL-27RA can activate STATs via their own intracellular tails (Nicola and Babon, 2015; Hermanns, 2015; Murakami et al., 2019). The patients' truncated GP130 mutant proteins can probably form high-affinity IL-27, LIF, and OSM receptors. The formation of

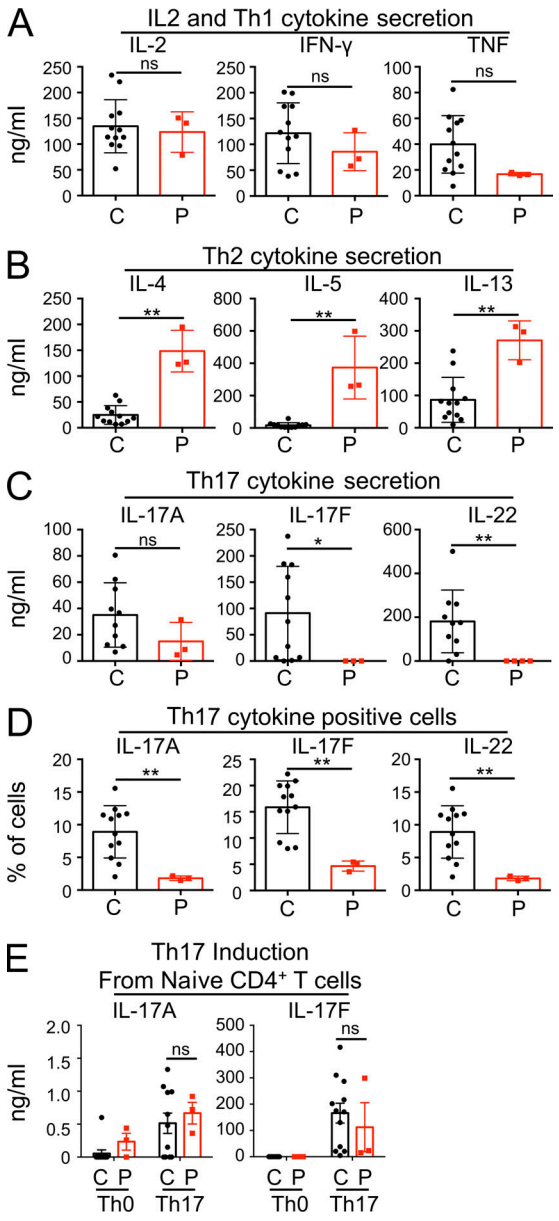


Figure 8. **In vitro functional assays of CD4⁺ Th cells. (A–C)** Secretion (ng/ml) of IL-2, Th1 (IFN-γ and TNF; A), Th2 (IL-4, IL-5, and IL-13; B), and Th17 (IL-17A, IL-17F, and IL-22; C) cytokines by memory CD4⁺ T cells after 5 d of stimulation with anti-CD2/CD3/CD28 mAb-coated beads. C, control; P, patients. **(D)** Frequency of Th17 (IL-17A, IL-17F, and IL-22) cytokine-positive memory CD4⁺ T cells after 4 d of culture under Th0 conditions (anti-CD3/CD2/CD28 antibody-coated beads). **(E)** Secretion (ng/ml) of Th17 (IL-17A and IL-17F) cytokines by naive CD4⁺ T cells after 5 d of culture under Th0 cell–polarizing conditions (anti-CD2/CD3/CD28 mAb-coated beads) or Th17 cell–polarizing conditions (anti-CD2/CD3/CD28 mAb-coated beads together with IL-1β, IL-6, IL-21, IL-23, and TGF-β). Mann–Whitney tests were used for all comparisons. ns, not significant. *, $P < 0.05$; **, $P < 0.01$.

high-affinity receptors, coupled with the intrinsic signaling capacity of the coreceptor, probably explains the weak but detectable STAT1 or STAT3 phosphorylation in HEK-GP130-KO cells transfected with the GP130 mutants and stimulated with IL-27, LIF, or OSM (Fig. S1, D and E). Consistently, IL-27–induced luciferase activity is not completely impaired in HEK-GP130-KO cells transfected with these mutants (Fig. 2 E and Fig. S2 A). We also observed weak luciferase activity following the stimulation, with LIF and OSM, of HEK-GP130-KO cells transfected with the EV, consistent with the weak affinity of LIF and OSM for LIF-R and OSM-R and the intrinsic signaling capacity of these two receptors (Fig. 2 E and Fig. S2 A; Nicola and Babon, 2015; Hermanns, 2015; Murakami et al., 2019). However, surprisingly, we did not detect an enhancement of luciferase responses to LIF or OSM in HEK-GP130-KO cells transfected with a truncated GP130 mutant from HIES patients relative to cells transfected with an EV. This suggests that the formation of high-affinity trimers with a truncated GP130 did not significantly enhance the signal over that for the low-affinity dimers formed between LIF or OSM and LIF-R or OSM-R.

The strongest DN effects of the mutant GP130 proteins against IL-6 and IL-11 signaling are explained in part by the coreceptors' lack of intrinsic signaling ability. It can also be explained by the valence of the multimers formed and/or the accumulation of DN GP130 mutant proteins at the cell surface. IL-6, IL-6R, and GP130 or IL-11, IL-11R, and GP130 form hexamers with a 2:2:2 stoichiometry essential for signal transduction (Murakami et al., 1993; Barton et al., 2000). By contrast, IL-27, LIF, and OSM form trimers with GP130 and their coreceptors (Gearing et al., 1992; Mosley et al., 1996; Pflanz et al., 2004). If each trimer requires one functional GP130 molecule and each hexamer requires two such molecules to transduce a signal, then a stronger DN effect would be expected for hexamers (Fig. 10, A and B). This phenomenon is probably amplified by the greater accumulation of mutant GP130 proteins in some cell types (e.g., HEK293T, monocytes, and fibroblasts) than in others (Fig. 10 C). For example, at a Mut:WT ratio of 1:1, 50% of trimers but only 25% of hexamers are functional. At a ratio of 4:1, 20% of trimers but only 4% of hexamers are functional. Consequently, the DN effect is stronger against IL-6 and IL-11 than against LIF, accounting for the patients having the HIES-AD phenotype rather than SWS. Intriguingly, however, the mutants lacking all four STAT3-binding sites have a DN effect on IL-6/IL-6Rα stimulation (trans-signaling) only at a very high Mut:WT ratio (8:1), whereas they have a strong DN effect on IL-6 stimulation alone (classic signaling) at a low Mut:WT ratio (e.g., 1:1). Co-transfection with IL-6R weakened the DN effect of the GP130 mutants in response to IL-6 alone. This suggests that a limited pool of membrane-anchored coreceptors exacerbate the DN effect. In other words, a critical activation threshold is less likely to be reached if the coreceptors are limiting because of competition for accessibility.

Even though the T761fs mutant has lost all four STAT3-binding domains and the recycling motif, it is the only HIES-causing mutant in which the tyrosine 759 (Y759) residue is retained. Upon phosphorylation, Y759 acts as a docking site for SOCS3, which switches off STAT3 activation (Nicholson et al., 2000; Schmitz et al., 2000). The knock-in mouse line expressing human GP130 with a homozygous Y759F mutation has splenomegaly, lymphadenopathy, enhanced acute-phase reactions, and prolonged STAT3 activation (Ohtani et al., 2000). Moreover, Y759 acts as a docking site for SHP2, triggering the second pathway of GP130 activation through MAPK (Fukada et al., 1996;

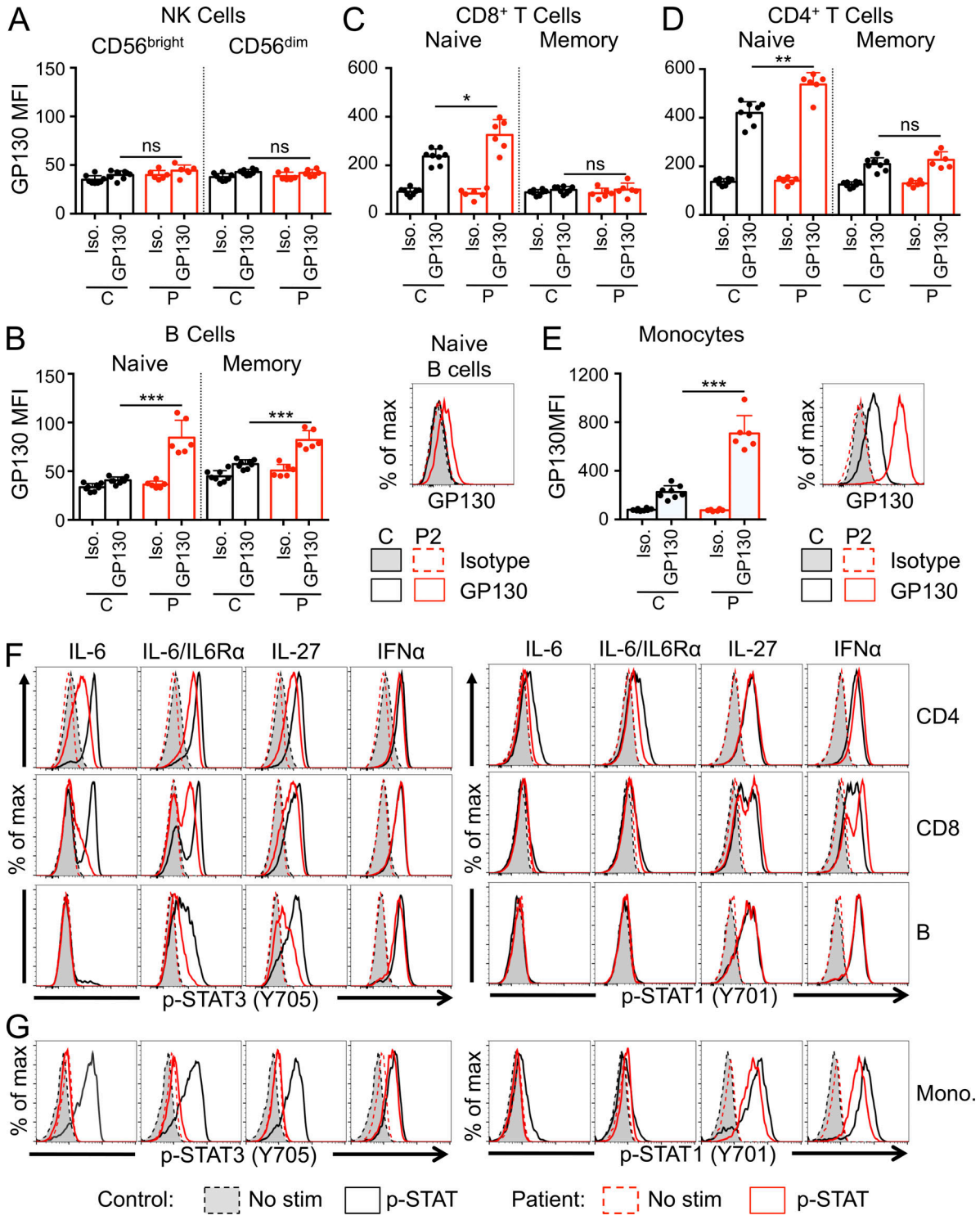


Figure 9. **GP130 production and activity in primary lymphocytes and monocytes from patients. (A–E)** GP130 levels, as evaluated by flow cytometry, in primary CD56$^{bright}$ and CD56$^{dim}$ NK cell subsets (A), naive and memory B cells (B), naive and memory CD8$^{+}$ T cells (C), naive and memory CD4$^{+}$ T cells (D), and monocytes (E). The graphs show the MFI of GP130, as measured by flow cytometry, in eight controls (C) and six patients (P2–P7). Representative data for GP130 expression in naive B cells (B) and monocytes (E) from P2 and a healthy control are shown, together with data for the isotypic control. **(A–E)** *t* tests were used for all comparisons. **(F)** PBMCs from P6 (red lines) and a control (black lines) were stimulated for 15 min with IL-6, IL-6/IL-6Rα, IL-27, or IFN-α or left unstimulated, and the phosphorylation of STAT3 (pY705) and STAT1 (pY701) was then evaluated in the indicated subsets. **(G)** Purified monocytes from P5 (red lines) and a control (black lines) were stimulated for 15 min with IL-6, IL-6/IL-6Rα, IL-27, or IFN-α or left unstimulated, and the phosphorylation of STAT3 (pY705) and STAT1 (pY701) was then evaluated. ns, not significant.

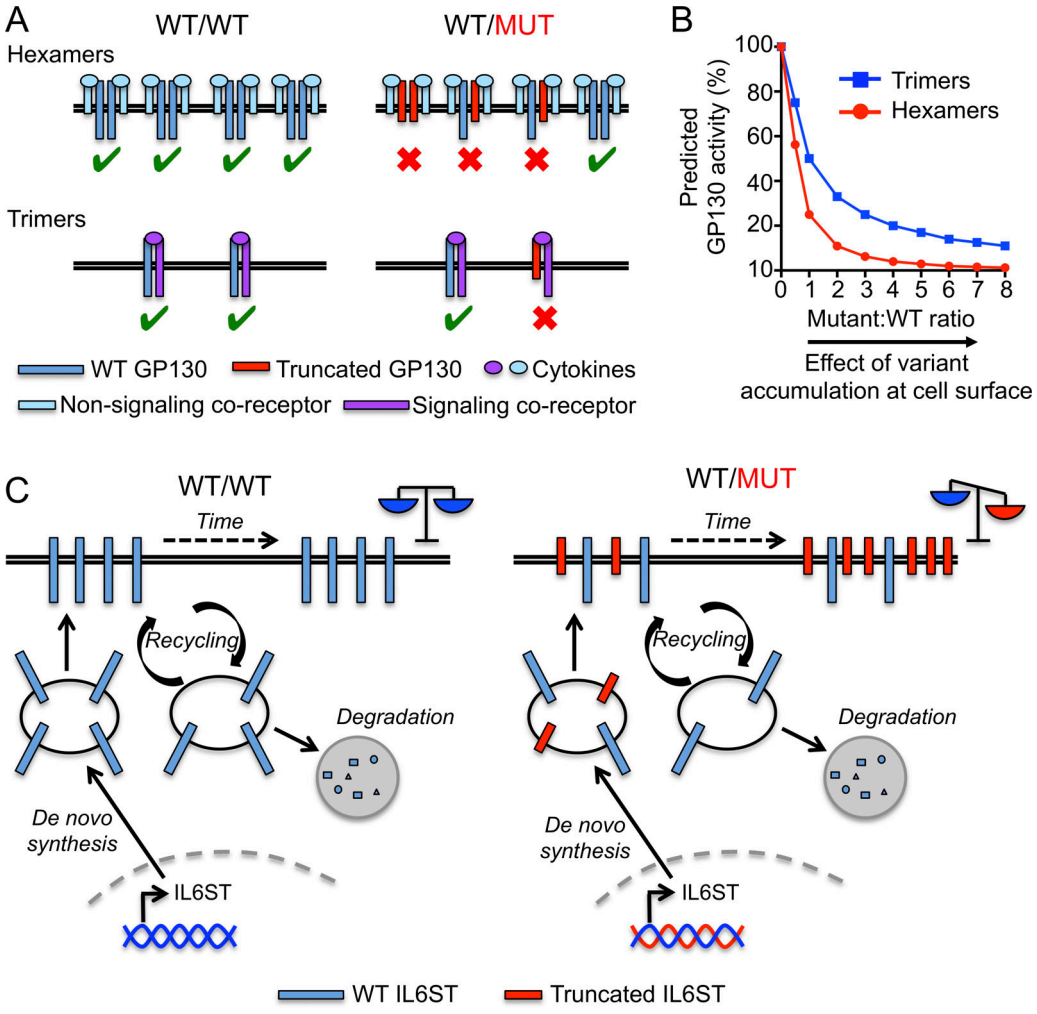


Figure 10. ***IL6ST* DN mutation mechanism of action. (A)** At a 1:1 Mut:WT ratio, truncated GP130 is predicted to impair 75% of GP130 downstream signaling hexamers (IL-6/IL-6R/GP130 or IL-11/IL-11RA/GP130) and 50% of GP130 downstream signaling trimers (IL-27/IL-27RA/GP130, LIF/LIF-R/GP130, or OSM/OSM-R/GP130). **(B)** The accumulation of mutant GP130 is predicted to have a stronger impact on IL-6 family cytokines forming hexamers (IL-6 and IL-11) than on those forming trimers (IL-27, LIF, and OSM) with GP130. **(C)** Mechanism of GP130 accumulation at the cell surface. Due to the missing recycling motif, truncated GP130 is not recycled in the basal state, unlike WT GP130. As a result, in heterozygous individuals, truncated GP130 is predicted to accumulate at the cell surface, whereas WT GP130 is predicted to be stably expressed due to a balance between de novo production and proteosomal degradation.

Nakajima et al., 1996; Yamanaka et al., 1996). Interestingly, the ability of GP130 mutants lacking all four STAT3 binding sites but retaining the Y759 motif to activate the MAPK pathway has been tested (Lehmann et al., 2003). These mutants were shown to retain their ability to activate the MAPK pathway, unlike mutants lacking Y759 and all four STAT3-binding sites. Consistent with these findings, the T761fs mutant of kindred A, the only mutant retaining Y759 in our series of HIES kindreds with AD GP130 deficiency, was able to activate the MAPK pathway. It may be no coincidence that kindred A had the mildest phenotype, with few, if any infections. On a related note, there are 13 predicted heterozygous LOF mutations of this gene in gnomAD, 9 of which are predicted to impair cell surface expression and not act in a DN manner. The other four predicted heterozygous LOF mutants lack one, two, or three STAT3-binding domains. None of these LOF mutants lack all four STAT3 domains, and none lack the recycling domain. At odds with our initial prediction, at least two of the three mutants tested (S789* and E899fs) are LOF and DN for cellular responses to IL-6 and IL-11 in vitro. However, the DN effect is milder than that of HIES-causing mutants, probably because these two mutants retain the recycling motif and at least one STAT3-binding site. It is tempting to speculate that these two variants are associated with clinical phenotypes milder than full-blown HIES. Nevertheless, it will be important to compare the biological and clinical phenotypes of patients with AD STAT3, AR ZNF341, and AR and AD partial GP130 deficiencies carefully, as these deficiencies all impair at least STAT3-dependent responses to IL-6 and IL-11 and seem to be clinical phenocopies, but not necessarily strict ones.

## Materials and methods

### Case reports

P1 (kindred A, Fig. 1 A) was born to nonconsanguineous French/Greek parents. He is the father of P2 and the grandfather of P3 and P4. He suffered from asthma associated with mild but

recurrent skin infections. No recent biological or clinical data are available for P1, and it was not therefore possible to calculate an National Institutes of Health (NIH) HIES score (Grimbacher et al., 1999b).

P2 (kindred A, Fig. 1 A) was born in 1972 and is the only child of nonconsanguineous French parents. He is currently 47 yr old. He is the son of P1 and father of P3 and P4. P2 has had eczema since early childhood, which improved when he reached adulthood. Complete deciduous tooth retention was successfully treated at the age of ∼20 yr. P2 has mild facial dysmorphism resembling that of HIES due to heterozygous *STAT3* mutations and scoliosis with a Cobb angle of 11° at the age of 44 yr. He has hyperextensible ankles and shoulders and has suffered numerous ankle sprains and shoulder dislocations. He has never suffered from bone fractures, and bone densitometry results were normal. He has never had candidiasis or pulmonary infections but reported delayed healing of cutaneous injuries, requiring the use of antibiotics. P2 has no allergies, and has an NIH HIES score of 27 (Grimbacher et al., 1999b).

P3 and P4 (kindred A, Fig. 1 A) were born in 2003 and 2006 and are currently 16 and 13 yr old, respectively. They are the son and daughter of P2. P3 was born at 8 mo of pregnancy and had a neonatal infection requiring intensive care. He had numerous ear, nose, and bronchial infections during the first 6 yr of life. Infections stopped after the initiation of prophylactic trimethoprim/sulfamethoxazole. P3 has no facial dysmorphism but presented a retention of deciduous teeth, which were surgically removed. He had mild eczema requiring intermittent treatment with topical steroids. He has never had skin abscesses or candidiasis. He has moderate scoliosis and hyperextensibility, resulting in frequent shoulder dislocations. He fractured his right humerus in a fall from his bike. He had pneumonia at the age of 13 yr, which was caused by *H. influenzae* and required intravenous antibiotics. Chest computed tomography (CT) showed a complete resolution of this episode, without the development of bronchiectasis or pneumatocele. Chest CT also revealed bronchomalacia of the left stump bronchus (Fig. 1 B). The NIH HIES score of P3 was 29. P4 is the sister of P3, and the daughter of P2. She was born at term and had to be hospitalized at the age of 1 yr for osteomyelitis of the wrist. She recovered, without parenchymal sequelae, from single pneumonia with concomitant herpes zoster infection in 2015. She displays mild facial dysmorphism, had to have several deciduous teeth removed surgically, and has moderate eczema requiring topical treatment. The NIH HIES score of P4 is 20 (Grimbacher et al., 1999b).

P5 (kindred B, Fig. 1 A) was born in France in 1993 to nonconsanguineous parents and is currently 26 yr old. P5 is of admixed French and North African descent. He was born at term without complications. He has suffered from asthma and bronchiectasis since the age of 4 yr. He reported *Staphylococcus aureus* lung infection at the age of ∼10 yr. In 2010, at the age of 17 yr, he presented with hemoptysis. Chest CT showed bilateral bronchiectasis. Between 2011 and 2017, his respiratory condition progressively worsened. In 2016, chest CT showed cylindrical and cystic bronchiectasis in the upper lobes, mainly in the right upper lobe. In January 2017, he was admitted for a lung abscess caused by *Escherichia coli*, resulting in a large persistent pneumatocele in the right upper lobe (Fig. 1 B). In August 2017, chronic pulmonary aspergillosis was diagnosed on the basis of very high anti-*Aspergillus* precipitin levels, a thickening of the cavity wall, and the appearance of a fungal ball on chest CT, which was treated with voriconazole. Imaging also showed a worsening of cystic bronchiectasis in the left upper and right lower lobes. HIES was suspected, and immunoglobulin substitution and cotrimoxazole prophylaxis were initiated. In March 2019, P5 was admitted for hemoptysis related to uncontrolled pulmonary aspergillosis. Liposomal amphotericin B and caspofungin replaced the previous treatment. Susceptibility tests on the *Aspergillus fumigatus* strain isolated from the patient revealed resistance to itraconazole, voriconazole, and isavuconazole due to a TR34/L98H mutation of *cyp51A*. Caspofungin and posaconazole replaced the previous treatment. The patient also experienced multiple bacterial superinfections of the pneumatocele after its formation. Pulmonary function tests in June 2019 showed severe obstructive lung disease resulting in a forced expiratory volume in 1 s of 1.1 liter or 27% the predicted value, with pronounced hyperinflation. P5 has never suffered from eczema, skin infections, or CMC. He has suffered from allergic rhinitis, and skin prick test results were positive for house dust mite and *Alternaria*. P5 has no facial dysmorphism but does have hyperextensible thumbs. A clubfoot was surgically corrected when the patient was 1 yr old. P5 displayed deciduous tooth retention, requiring the surgical extraction of 24 supernumerary teeth. From the age of 12 yr, he developed scoliosis, necessitating orthopedic care (Fig. 1 B). In 2017, he broke two ribs while coughing. Bone densitometry in 2018 demonstrated osteoporosis. The NIH HIES score of P5 is 48 (Grimbacher et al., 1999b).

P6 (kindred C, Fig. 1 A) was born in 1980 to second-cousin parents and is currently 39 yr old. P6 and his wife are of Bulgarian descent. P6 is the father of P7. He presented with severe eczema, allergic asthma, recurrent upper and lower respiratory tract infections, diffuse severe cystic bronchiectasis and recurrent bacterial skin abscesses requiring drainage during childhood and adolescence. Since 2012, he has suffered from allergic bronchopulmonary aspergillosis with high levels of *Aspergillus*-specific antibodies (IgE and IgG), managed with long-term oral steroid treatment. Skin prick tests were positive for *A. fumigatus* and *Alternaria*. At the age of 25 yr, P6 presented with massive hemoptysis related to combined cavitary pulmonary aspergillosis and mucormycosis in a large bronchiectasis cavity in the right upper lobe. Both *A. fumigatus* and fungi from the order Mucorales were isolated from respiratory secretions, and the patient was successfully treated with posaconazole for 3 yr. Even after the cessation of oral corticosteroid treatment, profound hypogammaglobulinemia persisted, with low levels of the IgG2 and IgG3 subclasses and IgA deficiency. Weekly subcutaneous immunoglobulin treatment was initiated; the specific pneumococcal antibody response was not assessed. Other pathogens, such as *Pseudomonas aeruginosa*, *H. influenzae*, and *S. aureus*, are frequently isolated from the patient's sputum, leading to frequent exacerbations of his underlying bronchiectasis. In 2019, the patient was readmitted with hemoptysis related to a relapse of *A. fumigatus* superinfection of the largest cavity in the right upper lobe and an endobronchial fungal ball in the left lung, both

confirmed by a high galactomannan antigen load and the detection of *A. fumigatus* in PCR tests on bronchoalveolar lavage fluid. The severe hemoptysis necessitated bronchial artery embolization and the prompt reinitiation of antifungal treatment with voriconazole. P6 has frontal bossing and supernumerary teeth, which were either retained or shed late. He smoked daily until 8 yr ago. The NIH HIES score of P6 is 47 (Grimbacher et al., 1999b).

P7 (kindred C, Fig. 1 A) was born in 2007 to nonconsanguineous parents and is currently 12 yr old. P7 is the daughter of P6. She suffers from atopic eczema, severe allergic asthma, and recurrent otitis, sinusitis, and bronchitis. She presented with left upper lobe pneumonia. Chest CT showed chronic bronchitis without bronchiectasis. She is allergic to house dust mite, grass, animals, and some foods (cow's milk and eggs), without anaphylactic reactions. She presented with recurrent bacterial skin infections without abscesses. Like her father, she has supernumerary teeth, and she shed her deciduous teeth late. She has no frontal bossing and no facial dysmorphism but a high palate. Unlike her father, she has normal serum total IgG and IgG subclass levels and normal antibody responses to both nonconjugated and conjugated vaccines. The NIH HIES score of P7 was 37 (Grimbacher et al., 1999b).

P8 (kindred D, Fig. 1 A) was born to nonconsanguineous parents and is currently 25 yr old. P8 is of Slovak descent. A clinical case report relating to P8 has been published (Boeck et al., 2001). Both P8 and his mother suffer from Saethre–Chotzen syndrome due to a heterozygous deletion in *TWIST*. However P8 also presented HIES, and because an immune phenotype has never been reported in TWIST patients, he was suspected to have a second genetic defect. Recurrent infections, severe staphylococcal pneumonia, purulent lymphadenitis, and conjunctivitis were noted during the patient's first 18 mo of life. Repeated staphylococcal abscesses were found, predominantly in the groin (Fig. 1 B). P8 also had staphylococcal abscesses in the neck, eventually leading to the removal of multiple lymph nodes at the age of 5 yr. P8 also suffered from mild eczema on the chest, face, and hands. His IgE level was regularly >10,000 IU/ml. The NIH HIES score of P8 was 38 (Grimbacher et al., 1999b).

P9 (kindred E, Fig. 1 A) was born in 1992 to nonconsanguineous parents and was 27 yr old at the time of her death from overwhelming pulmonary infection. She was half Mexican and half Salvadoran. She suffered from recurrent infections, including onychomycosis, five episodes of shingles between the ages of 2 and 20 yr, and recurrent otitis, pharyngitis, sinusitis, and bronchopulmonary infections. She reported 12 episodes of lung infection before the age of 13 yr and frequently required antibiotics thereafter. At the age of 13 yr, she suffered pneumonia complicated by empyema requiring chest drainage. From the age of 24 yr, she was hospitalized on multiple occasions for recurrent (despite partial pneumonectomy) right multifocal pneumonia resulting in multiple cystic and cavitary lesions (Fig. 1 B). She underwent endoscopic sinus surgery (Fig. 1 B), leading to an improvement in nasal symptoms, and culture demonstrated *Aspergillus* infection. Additional infections included pyelonephritis, with *E. coli* growing in cultures, at the age of 20 yr, and right foot cellulitis progressing to abscess and requiring incision, drainage, and intravenous antibiotics at the age of 22 yr. At the age of 23 yr, the patient suffered a left ankle fracture after twisting her ankle while walking in heels. The fracture required surgery, which was then complicated by *S. aureus* infection requiring incision, drainage, and intravenous antibiotics. The patient had a high palate, deciduous tooth retention, joint hyperextensibility, and scoliosis. She did not have craniosynostosis. She suffered from asthma and was treated with oral steroids on multiple occasions annually. She suffered from eczema and allergic rhinitis. The NIH HIES score of P9 was 66 (Grimbacher et al., 1999b).

P10 (kindred F, Fig. 1 A) was born in 1992 to nonconsanguineous Turkish parents. A clinical case report relating to P10 has been published (Saçilanateş et al., 2005). P10 suffered from pustular skin lesions from the age of 1 wk, with umbilical cord separation at 16 d. She had severe atopic dermatitis and recurrent sinopulmonary infections from the age of 6 mo. She had *S. aureus* pneumonia complicated by empyema requiring a chest tube at the age of 8 yr. She had several episodes of pneumonia between the ages of 8 and 10 yr, and pneumatocele was detected on chest CT. At the age of 10 yr, numerous cavities were detected, and she consulted for thoracic surgery for pneumatocele excision, the largest cavity being located in the left upper lobe. This patient had no facial dysmorphism or scoliosis. Her deciduous teeth fell out spontaneously, but late. She fractured her left humerus twice in falls. Physical examination revealed eczema, scars of old pustular lesions, hyperextensibility, and clubbing. P10 had eosinophilia and a total IgE level of 13,778 IU/ml. AD-HIES was suspected, so cotrimoxazole prophylaxis and immunoglobulin replacement therapy were initiated. At the age of 15 yr, P10 underwent surgery for a septated pneumatocele with a diameter of 8 × 5 × 8 cm in the left upper lobe. Pathology results were consistent with chronic fibrinous pleurisy with *Aspergillus* colonization. P10 was lost to follow up between 2007 and 2014 but received regular intravenous Ig (IVIg) treatment and cotrimoxazole prophylaxis. She was admitted to the local hospital for hemoptysis in 2012, and bleeding in the right bronchial and right intercostal arteries was controlled by embolization. In January 2014, at the age of 22 yr, she was admitted for hemoptysis of 2 mo duration. Chest CT showed a severe worsening of the condition of the lung parenchyma (Fig. 1 B), with images consistent with bleeding in the right lung, upper lobe anterior cyst, and bronchus dilation. Thoracic aortography and bronchial arteriography were performed, and active hemorrhaging was detected in both bronchial arteries. Embolization was performed on all bleeding arteries. P10 was intubated and evaluated for lung transplantation. Her clinical condition deteriorated within 2 wk, and extracorporeal membrane oxygenation support was provided. She died before lung transplantation. The NIH HIES score of P10 was 52 (Grimbacher et al., 1999b).

P11 (kindred G, Fig. 1 A) was born in 2001 to nonconsanguineous American parents and is currently 18 yr old. P11 is of European descent. He has had allergic rhinitis and mild asthma since early childhood, controlled with inhaled fluticasone and, when required, albuterol. At the age of 9 yr, he presented with a cough of a few months' duration and acute fever.

Chest imaging revealed a large cavitary lesion, bronchiectasis, and patches of infiltrate, and bronchoalveolar lavage was positive for *A. fumigatus*. Antifungal drugs were therefore initiated. Approximately 4 mo after initial presentation, he developed spontaneous pneumothorax complicated by a persistent bronchopleural fistula. Allergic bronchopulmonary aspergillosis was diagnosed, and the patient was treated with intermittent corticosteroids for flare-ups and was included in an omalizumab trial. The patient also has a history of esophagitis, primary tooth retention requiring the extraction of eight teeth, wrist fracture, and arthralgia. P11 has no full siblings, but two half siblings and the parents of this patient are healthy. He has two half siblings who are healthy. Serum IgG, IgA, and IgM levels have remained within normal limits, and specific antibodies against tetanus and pneumococcal were present. Serum IgE concentrations for this patient range from 250 to 13,000 IU/ml. The NIH HIES score of P11 is 52 (Grimbacher et al., 1999b).

P12 (kindred H, Fig. 1 A) was born in 1998 to nonconsanguineous American parents and is currently 22 yr old. P12 is of European descent. He was diagnosed with asthma at the age of 2 yr and had recurrent asthma exacerbations as a child. He had symptoms of mild nasal allergies but no eczema. Thirteen of his deciduous teeth were retained, and the patient displayed mild scoliosis that did not require treatment. He had recurrent and recalcitrant tinea pedis and one skin abscess. He received all routine childhood vaccines, including live vaccines, without adverse events. At the age of 12 yr, he had osteomyelitis of the elbow. The same year, he underwent bronchoscopy for recurrent pneumonia; *Aspergillus* was grown from the bronchoscopy specimen, leading to the patient being placed on prednisone and itraconazole. At the age of 17 yr, after multiple hospitalizations and chest tube placements, he was found to have bronchiectasis with invasive aspergillosis of the lungs and fungal invasion of the arteries and underwent right middle lobe and lower lobe resection. Treatment with itraconazole continued until the hospitalization of this patient in 2019 for hemoptysis and severe pneumonia (bronchoalveolar lavage showing *Aspergillus* and methicillin-sensitive *S. aureus*), with a chest CT scan showing finger-in-glove mucoid impaction and bronchiectasis. He is currently relatively stable as an outpatient for 6 mo, having completed his course of prednisone, on bactrim, voriconazole, and subcutaneous immunoglobulins. His IgE levels were high, and he was initially diagnosed with common variable immunodeficiency at the age of 18 yr (low IgG levels and a lack of specific antibody response). This patient did not develop pneumonia during 3 yr of IVIg treatment, but IVIg was stopped when he reached the age of 21 yr due to a lack of health insurance coverage. This patient's family history includes a father with severe, steroid-dependent asthma, rheumatoid arthritis, multiple infections, and diverticulitis requiring colostomy, who died at the age of 26 yr after prolonged hospitalization in an intensive care unit. The NIH HIES score of P12 is 44 (Grimbacher et al., 1999b).

The experiments described here were conducted in accordance with local, national, and international regulations and were approved by the French Ethics committee, French National Agency for Medicines and Health Product Safety, and the French Ministry of Research. Informed consent was obtained from all patients or their families, in the case of minors, in accordance with the World Medical Association, the Helsinki Declaration, and European Union directives.

### WES

WES was performed with individual institutional protocols. We extracted genomic DNA from blood samples collected from the patients and their parents and siblings with the iPrep PureLink gDNA Blood Kit and iPrep Instruments from Life Technologies. WES was performed for all patients except P1 and P7. Exome capture was performed with the SureSelect Human All Exon 71 Mb kit (Agilent Technologies). Paired-end sequencing was performed on a HiSeq 2500 machine (Illumina) generating 100-base reads. We aligned the sequences with the GRCh37 reference build of the human genome using the Burrows-Wheeler Aligner (Li and Durbin, 2010). Downstream processing and variant calling were performed with the Genome Analysis Toolkit (McKenna et al., 2010), SAMtools (Li et al., 2009), and Picard tools. Substitution and InDel calls were made with the GATK UnifiedGenotyper. All variants were annotated with annotation software developed in-house (Adzhubei et al., 2010; Kircher et al., 2014; Ng and Henikoff, 2001).

### Sanger sequencing

Genomic DNA was obtained from whole blood from patients. The *IL6ST* mutation was amplified from genomic DNA by PCR; the PCR products were purified by centrifugation through Sephadex G-50 Superfine resin (Amersham-Pharmacia-Biotech) and sequenced with the BigDye Terminator Cycle Sequencing Kit (Applied Biosystems). Sequencing products were purified by centrifugation through Sephadex G-50 Superfine resin, and sequences were analyzed with an ABI Prism 3500 apparatus (Applied Biosystems). The sequences obtained were aligned with the genomic sequence of *IL6ST* (Ensembl) with Serial Cloner 2.6 software.

### Cell culture

PBMCs were isolated by Ficoll-Hypaque centrifugation (Amersham-Pharmacia-Biotech) from cytopheresis or whole-blood samples obtained from healthy volunteers and patients, respectively. Primary human fibroblasts were isolated from a 5-mm skin punch biopsy or from surgical skin margins from healthy donors. Briefly, epidermis was separated from dermis by dispase (BD Bioscience) digestion overnight at +4°C, and the keratinocytes were isolated from the epidermis by scraping into a trypsin solution (Thermo Fisher Scientific). The dermis was cut into pieces and the explants were kept in DMEM supplemented with 10% fetal bovine serum (Sigma-Aldrich) for 10–15 d for fibroblast isolation. Primary fibroblasts and HEK293T cells were cultured in DMEM supplemented with 10% fetal bovine serum. EBV-B cell lines were maintained in RPMI 1640 supplemented with 10% fetal bovine serum (Sigma-Aldrich).

### Generation of GP130-deficient HEK293T cells

GP130-deficient HEK293T cells were generated with the CRISPR/Cas9 system. Guide RNAs were designed with the

Benchling design tool, and inserted into lentiCRISPR v2, which was a gift from Feng Zhang (plasmid #52961; Addgene). The guide RNAs (forward: 5′-CACCGTATGTACTTACTATCTTCAT-3′; reverse: 5′-AAACATGAAGATAGTAAGTACATAC-3′) were designed to bind to intron 8 and to cut in exon 8. Using X-tremeGENE 9 DNA Transfection Reagent (Roche), we transiently transfected WT HEK293T cells with the resulting plasmid and cultured them for 5 d in the presence of puromycin before sorting the GP130$^{-}$ cells. The resulting cell line was subsequently tested for impaired GP130 expression and function and normal STAT1 and STAT3 expression.

### Plasmids and transient transfection

The C-terminal Myc/DDK-tagged pCMV6 EV, the human *IL6ST*, and *IL6R* expression vectors were purchased from Origene. Constructs carrying mutant alleles were generated by direct mutagenesis with the QuikChange II XL Site-Directed Mutagenesis Kit (Agilent Technologies), according to the manufacturer's instructions. A stop codon was introduced by mutagenesis between the *IL6ST* cDNA and the Myc/DDK tag. HEK293T cells were transiently transfected with the various constructs, with X-tremeGENE 9 DNA Transfection Reagent (Roche), used according to the manufacturer's instructions.

### Cell lysis, PNGase F treatment, and immunoblotting

For overexpression experiments, GP130-deficient HEK293T cells were cotransfected with a WT or mutant pCMV6-GP130 vector or an empty pCMV6 vector and cultured for 24 h before harvesting and cell lysis. Total protein extracts were prepared by mixing cells with lysis buffer (50 mM Tris, pH 7.4, 150 mM NaCl, 2 mM EDTA, and 0.5% Triton X-100) and incubating for 30 min at 4°C. The cells were centrifuged for 10 min at 16,000 ×*g*, and the supernatant was collected for immunoblotting. A mixture of protease and phosphatase inhibitors was added to the buffers immediately before use: aprotinin (10 µg/ml; Sigma-Aldrich), PMSF (1 mM; Sigma-Aldrich), leupeptin (10 µg/ml; Sigma-Aldrich), protease inhibitor cocktail (1×; Sigma-Aldrich). DNA was digested with Pierce Universal Nuclease for Cell Lysis (1/100; Thermo Fisher Scientific) during the lysis step. When indicated, PNGase F treatment was used in accordance with the manufacturer's instructions (New England Biolabs) to eliminate N-glycosylation. The proteins were separated by SDS-PAGE and immunoblotting was performed with antibodies against GP130 (E-8; Santa Cruz) and GAPDH (FL335; Santa Cruz).

### Immunophenotyping

Immunophenotyping was performed by flow cytometry, with mAbs against CCR7 (G043H7; Sony), CD1c (L161; BioLegend), CD3 (7D6; Invitrogen; UCHT1; BD), CD4 (RPA-T4; BD), CD8 (RPA-T8; BD), CD11c (S-HCL-13; BD), CD14 (M5E2; BD), CD16 (3G8; BD), CD19 (4G7, BD), CD20 (LT20; Miltenyi Biotec), CD25 (MA-251; BD), CD27 (O323; Sony; L128; BD), CD45RA (Hl100; BD), CD56 (B159; BD; NCAM16.2; BD), CD123 (6H6; BioLegend), CD130/GP130 (AM64; BD), CD141 (1A4; BD), CD161 (DX12; BD), CD183 (G025H7; BioLegend), CD185/CXCR5 (REA103; Miltenyi Biotec), CD194/CCR4 (REA279; Miltenyi Biotec), CD196/CCR6 (REA190; Miltenyi Biotec) FOXP3 (259D/C7; BD), IgA (IS11-8E10; Miltenyi Biotec), IgG (G18-145; BD), IgM (PJ2-22H3; Miltenyi Biotec), KIR2DL1/S1 (EB6; Beckman Coulter) KIR2DL2/S2/L3 (GL183, Beckman Coulter), KIR3DL1 (DX9; BioLegend), NKG2A (REA110; Miltenyi Biotec), NKG2C (REA205; Miltenyi Biotec), TCR-iNKT (6B11; BD), TCR-γδ (11F2; Miltenyi Biotec), and TCR-Vα7.2 (REA179; Miltenyi Biotec). We assessed the expression of mutant and WT GP130 alleles in an overexpression system by transfecting a GP130-deficient HEK293T cell with an empty pCMV6 vector, or WT or mutant pCMV6-GP130, culturing for 48 h, and then detaching the cells by pipetting for extracellular GP130 staining. For the evaluation of GP130 expression in primary fibroblasts, adherent cells were washed in 1 × PBS and detached with trypsin for GP130 staining. Cells were also stained with the Aqua Live/Dead Cell Stain Kit (Thermo Fisher Scientific). Where indicated, primary fibroblasts were incubated with cycloheximide (10 µg/ml; Sigma-Aldrich) for the indicated time before staining for extracellular GP130 and with a dead cell marker. When required, for intracellular staining, cells were fixed and permeabilized with a fixation/permeabilization kit (eBioscience or BD) after extracellular staining. Samples were analyzed with a Fortessa X20 (BD), or Gallios (Beckman Coulter) flow cytometer, depending on the experiment. Data were then analyzed with FlowJo 10.5.3 software. The terminal differentiation profile of the CD56$^{dim}$ compartment was investigated by determining the distribution of NKG2A and KIR (Béziat et al., 2010; Björkström et al., 2010). P9 immunophenotyping was performed as previously described (Shahin et al., 2019).

### Cytokines

IL-6, IL-11, LIF, and OSM were purchased from Miltenyi Biotech. The IL-6–IL-6Rα fusion protein and IL-27 were purchased from R&D Systems. IFN-α (Intron A) was purchased from Merck. IL-6, IL-6–IL-6Rα, IL-11, IL-27, LIF, and OSM were all used at a final concentration of 100 ng/ml. IFN-α was used at a final concentration of $10^5$ U/ml.

### Luciferase reporter assay

Reporter assays were performed as previously described (Béziat et al., 2018). GP130-deficient HEK293T cells were plated for 24 h before transfection in DMEM supplemented with 10% FCS. We assessed the impact of the mutation on GP130 function by transfecting cells with the pGL4.47{luc2P/SIE/Hygro} (Promega) reporter plasmids (100 ng/well for a 96-well plate), the pRL-SV40 vector (40 ng/well), and a WT or mutant pCMV6-GP130 (100 ng/well) in the presence of X-tremeGENE 9 DNA Transfection Reagent (Roche). We assessed the DN effect of each mutant allele by transfecting GP130-deficient HEK293T cells with the pGL4.47{luc2P/SIE/Hygro} (Promega) reporter plasmids (100 ng/well for a 96-well plate), the pRL-SV40 vector (40 ng/well), the WT pCMV6-GP130 (25 ng/well), and various concentrations of mutant pCMV6-GP130 (12.5 ng/well, 25 ng/well, 50 ng/well, 100 ng/well, or 200 ng/well) in the presence of X-tremeGENE 9 DNA Transfection Reagent (Roche). In the DN assays, wells transfected with the pGL4.47{luc2P/SIE/Hygro} (Promega) reporter plasmids (100 ng/well for a 96-well plate), the pRL-SV40 vector (40 ng/well), and the WT pCMV6-GP130 only (25 ng/well) or the indicated mutant pCMV6-GP130 only

(200 ng/well) or the empty pCMV6 only (200 ng/well) were also included as controls. The DNA content of each well was made up to 365 ng/well with empty pCMV6 vector to ensure that each well contained the same amount of DNA. For IL-6R cotransfection luciferase experiments, we used 25 ng of the WT pCMV6-*IL6R* and 25 ng of the WT and I719fs pCMV6-*IL6ST* plasmids in the indicated wells. The DNA content of each well was made up to 215 ng/well with empty pCMV6 vector to ensure that each well contained the same amount of DNA. The medium was removed 24 h after transfection and replaced with DMEM supplemented with 10% FCS and the indicated cytokines. Experiments were performed with technical duplicates and the promoter activity of each well is expressed as firefly luciferase activity/*Renilla* luciferase activity.

### CD4$^+$ T cell isolation and functional characterization

PBMCs were incubated with mAbs against CD4, CD45RA, CCR7, CD127, and CD25. Naive and memory CD4$^+$ T cells were isolated by first excluding T reg cells (CD25$^{hi}$CD127$^{lo}$) and then sorting CD4$^+$CD45RA$^+$CCR7$^+$ or CD4$^+$CD45RA$^-$CXCR5$^-$CCR7$^{+/-}$ cells, respectively. Isolated naive and memory CD4$^+$ T cells were then cultured in 96-well round-bottomed (30–40 × 10$^3$ cells/well) with T cell activation and expansion beads (coated with mAbs against CD2/CD3/CD28; Miltenyi Biotech) alone (Th0) or under Th17 cell–polarizing conditions. After 5 d, supernatants were harvested and the production of IL-4, IL-5, IL-9, IL-10, IL-13, IL-17A, IL-17F, and IFN-γ was determined by cytometric bead arrays (Becton Dickinson); IL-22 secretion was measured by ELISA (eBioscience). For cytokine expression, activated CD4$^+$ T cells were restimulated with PMA (100 ng/ml)/ionomycin (750 ng/ml) for 6 h, with brefeldin A (10 µg/ml) added after 2 h. Cells were then fixed, and the intracellular levels of IL-4, IL-9, IL-13, IL-10, IL-17A, IL-17F, IL-22, IL-21, and IFN-γ were determined.

### Phospho-STAT (p-STAT) and ERK experiments

Primary fibroblasts were cultured in DMEM-2% FCS for 16 h and then in DMEM-0% FCS for 2 h before the assays. For p-STAT experiments, GP130-deficient HEK293T cells were cultured in DMEM-10% FCS for 16 h before transfection with the WT or mutant pCMV6-GP130 or empty pCMV6, and were then cultured for a further 24 h before the assay. For p-ERK1/2 experiments, GP130-deficient HEK293T cells were cultured in DMEM-10% FCS for 16 h before transfection with the WT or mutant pCMV6-GP130 or empty pCMV6, were then cultured for 24 h in DMEM-10% FCS, and starved of serum in DMEM-0.5% FCS for a further 16 h before the assay. Monocyte experiments were performed with cells purified from fresh PBMCs (CD14 MicroBeads, Miltenyi Biotec), which were allowed to rest for 2 h at 37°C in RPMI-2% FCS before the assay. Experiments with B cells and CD4$^+$ and CD8$^+$ T cells were performed with freshly isolated PBMCs rested overnight in X-VIVO 20 serum-free medium (Lonza). Levels of p-STAT3 in EBV-B cells were determined in serum-starved cells, which were then stimulated with IL-6 (50 ng/ml), IL-27 (40 ng/ml), and IL-21 (50 ng/ml) before fixation. Except for primary fibroblasts and GP130-deficient HEK293T cells, cells were stained with Aqua Dead cell marker (Thermo Fisher Scientific) or Fixable Viability Dye eFluor 780 (eBioscience) before incubation with the indicated cytokines for 15 min in the corresponding medium, fixation in Fix buffer I (1:1 volume; BD Biosciences), and incubation for 10 min at 37°C. Primary fibroblasts and GP130-deficient HEK293T cells were incubated with the indicated cytokines for 15 min. The medium was then removed and the fibroblasts were washed once with 1 × PBS to remove dead cells. Adherent fibroblasts and GP130-deficient HEK293T cells were recovered by treatment with trypsin and were washed once in cold medium before fixation by incubation for 10 min with Fix buffer I. When required for the analysis of lymphocyte subsets, cells were stained for extracellular epitopes, including CD4 (RPA-T4, BD), CD8 (BW135/80, Miltenyi Biotech), and CD3 (Bw264/56; Miltenyi Biotech) before permeabilization. Cells were then permeabilized by incubation for 20 min at room temperature in Perm buffer III (BD Biosciences) and stained for 3 h at 4°C with anti-STAT3-pY705 (4/P-STAT3; BD), anti-STAT1-pY701 (14/P-STAT1), anti-ERK1/2-pT202/pY204 (20A), or isotypic control antibody. When required for the analysis of primary B cells, CD20 (H1; BD) was added together with anti-p-STAT antibodies. Cells were analyzed on a FACS Gallios machine.

### Statistics

Two-tailed Mann–Whitney tests were used for single comparisons of independent groups. In the relevant figures, ****, $P < 0.0001$; ***, $P < 0.001$; **, $P < 0.01$; and *, $P < 0.05$. Analyses were performed with GraphPad software.

### Online supplemental material

Fig. S1 shows expression of the GP130 mutants and phosphorylation assays of STAT1 and STAT3. Fig. S2 shows molecular characterization of the GP130 mutants. Fig. S3 shows an assay of the negative dominance of the GP130 mutants. Fig. S4 shows primary fibroblasts. Fig. S5 shows GP130 expression and function in PBMCs. Table S1 is a clinical summary of IL6ST-DN patients. Table S2 lists the biological parameters of patients with DN *IL6ST* mutations. Table S3 lists the biological parameters of patients with DN *IL6ST* mutations. Data S1 lists members of the Undiagnosed Diseases Network.

## Acknowledgments

We thank the patients and their families for participating in this study. We thank the members of the Human Genetics of Infectious Diseases laboratory for helpful discussions. We thank Yelena Nemirovskaya, Dominick Papandrea, Mark Woollett, Céline Desvallées, and Cécile Patissier for administrative assistance. We thank Lisa Roels, Veronique Debacker, and Nancy De Cabooter for excellent technical assistance and the VIB Flow Core for training, support, and access to the instrument park. We thank Drs. Zachary Marshall, Joud Hajjar, and Jennifer Posey for their evaluations.

This work was supported by the St. Giles Foundation; the Rockefeller University; Institut National de la Santé et de la Recherche Médicale; Paris Descartes University; the Howard Hughes Medical Institute; the Job Research Foundation; the French National Research Agency under the "Investissement d'avenir"

program (grant number ANR-10-IAHU-01), the "GENMSMD" project (grant ANR-16-CE17-0005-01 to L.-J. Couderc), the "LTh-MSMD-CMCD" project (grant ANR-18-CE93-0008-01), the "PNEUMOPID" project (grant ANR 14-CE15-0009-01), and the "HGDIFD" project (grant ANR-14-CE15-0006-01); the French Foundation for Medical Research (EQU201903007798); the Jeffrey Model Foundation; the Yale Center for Mendelian Genomics (UM1HG006504) funded by the National Human Genome Research Institute and the National Heart, Lung, and Blood Institute; the GSP Coordinating Center (U24 HG008956), which contributed to cross-program scientific initiatives and provided logistical and general study coordination; the NIH (grant R01AI127564); the National Center for Advancing Translational Sciences, NIH Clinical and Translational Science Award program (UL1 TR001866); the University Hospital Ghent Spearhead Initiative for Immunology Research; and the Grand Challenges Program of VIB. This VIB program received support from the Flemish Government under the Management Agreement 2017–2021 (VR 2016 2312 Doc.1521/4). T.A. Chatila is supported by NIH grant R01AI128976. B. Grimbacher is funded by the Deutsche Forschungsgemeinschaft: SFB1160/2_B5, under Germany's Excellence Strategy (CIBSS – EXC-2189 – Project ID 390939984; and RESIST – EXC 2155 – Project ID 39087428); through the European Joint Programme on Rare Diseases of the European Union, managed by Deutsche Forschungsgemeinschaft (grant GR1617/14-1/iPAD); and through the Bundesministerium für Bildung und Forschung (grant GAIN_ 01GM1910A). S.J. Tavernier is a postdoctoral fellow with the Fund for Scientific Research Flanders (FWO 1236920N). M.R.L. Maglorius Renkilaraj and J. Rosain are supported by Institut National de la Santé et de la Recherche Médicale. F. Haerynck was funded by a university research grant (BOF-University Ghent). V. Béziat was supported by the French National Research Agency (grant NKIRP-ANR-13-PDOC-0025-01). S.G. Tangye is supported by the National Health and Medical Research Council of Australia and the Job Research Foundation. H.H. Uhlig is supported by the Biomedical Research Centre BRC Oxford. H.H. Uhlig, A. Laurence, and Y.-H. Chen are supported by Celgene. The research reported in this manuscript was supported by the NIH Common Fund through the Office of Strategic Coordination/Office of the NIH director under award U01HG007709. The content is solely the responsibility of the authors and does not necessarily represent the official views of the NIH.

Author contributions: V. Béziat, S.G. Tangye, H.H. Uhlig, F. Haerynck, J.-L. Casanova, and A. Puel designed the study and wrote the manuscript. V. Béziat, S.J. Tavernier, Y.-H. Chen, C.S. Ma, M. Materna, A. Laurence, J. Staal, D. Aschenbrenner, L. Roels, L. Worley, K. Claes, L.-M. Charbonnier, J. Nammour, N. Vladikine, and M. Migaud performed the experiments. V. Béziat, M. De Bruyne, K. Schmitz-Abe, Y. Seeleuthner, H. Dai, L.C. Burrage, and D.R. Murdock conducted exome analyses. L.A. Kohn, S. Keles, M.R.L. Maglorius Renkilaraj, J. Rosain, M. Jeljeli, E. Van Braeckel, J.A. Rosenfeld, B.N. Lambrecht, V. Avettand-Fenoel, T.P. Vogel, C.R. Esther Jr., S. Haskologlu, F. Dogu, P. Ciznar, D. Boutboul, M. Ouachée-Chardin, J. Amourette, M.-N. Lebras, C. Gauvain, C. Tcherakian, A. Ikinciogullari, M.J. Butte, J.D. Milner, A.F. Freeman, B. Grimbacher, L.-J. Couderc, E. Catherinot, C. Fieschi, and T.A. Chatila provided material from the patients and conducted clinical exploration. B. Boisson, R. Beyaert, L. Abel, B. Grimbacher, and T.A. Chatila provided expertise and feedback. J.-L. Casanova and A. Puel secured funding. All the authors critically reviewed the manuscript.

Disclosures: Dr. Chen reported grants from Bristol-Myers Squibb during the conduct of the study. Dr. Rosenfeld reported personal fees from Baylor Genetics Laboratories outside the submitted work. Dr. Milner reported a patent to use STAT3 inhibition to prevent anaphylaxis pending. Dr. Couderc reported non-financial support from Astra Zeneca, personal fees from Boehringer Ingelheim, personal fees from Novartis, and grants from LVL outside the submitted work. Dr. Catherinot reported financial support for travel and registration expenses related to international medical meetings (LVL Medical, CSL Behring). Dr. Uhlig reported grants from Celgene during the conduct of the study and grants from UCB and Eli Lilly outside the submitted work. Dr. Haerynck reported, "Centre for Primary Immune deficiency is recognized as a Jeffrey Modell Foundation diagnostic and research center and supported by the Jeffrey Modell Foundation; the University Hospital Ghent Spearhead Initiative for Immunology Research (until 7/2019); the Grand Challenges Program of VIB (this VIB Program received support from the Flemish Government under the Management Agreement 2017-2021; VR 2016 2312 Doc.1521/4); Simon Tavernier is a postdoctoral fellow at PID research lab with the Fund for Scientific Research Flanders (FWO, 12W9119N); I am funded by a university research grant (BOF-University Ghent)." No other disclosures were reported.

Submitted: 25 September 2019
Revised: 14 January 2020
Accepted: 18 February 2020

## References

Adzhubei, I.A., S. Schmidt, L. Peshkin, V.E. Ramensky, A. Gerasimova, P. Bork, A.S. Kondrashov, and S.R. Sunyaev. 2010. A method and server for predicting damaging missense mutations. *Nat. Methods.* 7:248–249. https://doi.org/10.1038/nmeth0410-248

Arita, K., A.P. South, G. Hans-Filho, T.H. Sakuma, J. Lai-Cheong, S. Clements, M. Odashiro, D.N. Odashiro, G. Hans-Neto, N.R. Hans, et al. 2008. Oncostatin M receptor-β mutations underlie familial primary localized cutaneous amyloidosis. *Am. J. Hum. Genet.* 82:73–80. https://doi.org/10.1016/j.ajhg.2007.09.002

Avery, D.T., E.K. Deenick, C.S. Ma, S. Suryani, N. Simpson, G.Y. Chew, T.D. Chan, U. Palendira, J. Bustamante, S. Boisson-Dupuis, et al. 2010. B cell-intrinsic signaling through IL-21 receptor and STAT3 is required for establishing long-lived antibody responses in humans. *J. Exp. Med.* 207:155–171. https://doi.org/10.1084/jem.20091706

Barton, V.A., M.A. Hall, K.R. Hudson, and J.K. Heath. 2000. Interleukin-11 signals through the formation of a hexameric receptor complex. *J. Biol. Chem.* 275:36197–36203. https://doi.org/10.1074/jbc.M004648200

Bergerson, J.R.E., and A.F. Freeman. 2019. An Update on Syndromes with a Hyper-IgE Phenotype. *Immunol. Allergy Clin. North Am.* 39:49–61. https://doi.org/10.1016/j.iac.2018.08.007

Béziat, V., B. Descours, C. Parizot, P. Debré, and V. Vieillard. 2010. NK cell terminal differentiation: correlated stepwise decrease of NKG2A and acquisition of KIRs. *PLoS One.* 5:e11966. https://doi.org/10.1371/journal.pone.0011966

Béziat, V., J. Li, J.-X. Lin, C.S. Ma, P. Li, A. Bousfiha, I. Pellier, S. Zoghi, S. Baris, S. Keles, et al. 2018. A recessive form of hyper-IgE syndrome by disruption of ZNF341-dependent STAT3 transcription and activity. *Sci. Immunol.* 3:eaat4956. https://doi.org/10.1126/sciimmunol.aat4956

Björkström, N.K., P. Riese, F. Heuts, S. Andersson, C. Fauriat, M.A. Ivarsson, A.T. Björklund, M. Flodström-Tullberg, J. Michaëlsson, M.E. Rottenberg, et al. 2010. Expression patterns of NKG2A, KIR, and CD57 define a process of CD56dim NK-cell differentiation uncoupled from NK-cell education. *Blood.* 116:3853–3864. https://doi.org/10.1182/blood-2010-04-281675

Boeck, A., C. Kosan, P. Ciznar, and J. Kunz. 2001. Saethre-Chotzen syndrome and hyper IgE syndrome in a patient with a novel 11 bp deletion of the TWIST gene. *Am. J. Med. Genet.* 104:53–56. https://doi.org/10.1002/ajmg.10007

Buckley, R.H. 2020. Conversations with Founders of the Field of Human Inborn Errors of Immunity. *J. Clin. Immunol.* https://doi.org/10.1007/s10875-019-00736-y

Buckley, R.H., B.B. Wray, and E.Z. Belmaker. 1972. Extreme hyperimmunoglobulinemia E and undue susceptibility to infection. *Pediatrics.* 49:59–70.

Chandesris, M.-O., A. Azarine, K.-T. Ong, S. Taleb, P. Boutouyrie, E. Mousseaux, M. Romain, E. Bozec, S. Laurent, N. Boddaert, et al. 2012a. Frequent and widespread vascular abnormalities in human signal transducer and activator of transcription 3 deficiency. *Circ. Cardiovasc. Genet.* 5:25–34. https://doi.org/10.1161/CIRCGENETICS.111.961235

Chandesris, M.O., I. Melki, A. Natividad, A. Puel, C. Fieschi, L. Yun, C. Thumerelle, E. Oksenhendler, D. Boutboul, C. Thomas, et al. 2012b. Autosomal dominant STAT3 deficiency and hyper-IgE syndrome: molecular, cellular, and clinical features from a French national survey. *Medicine (Baltimore).* 91:e1–e19. https://doi.org/10.1097/MD.0b013e31825f95b9

Chen, Y.-H., G. Grigelioniene, P.T. Newton, J. Gullander, M. Elfving, A. Hammarsjö, D. Batkovskyte, H.S. Alsaif, W.I.Y. Kurdi, F. Abdulwahab, et al. 2020. Absence of GP130 cytokine receptor signaling causes extended Stüve-Wiedemann syndrome. *J. Exp. Med.* 217:e20191306. https://doi.org/10.1084/jem.20191306

Chérel, M., M. Sorel, B. Lebeau, S. Dubois, J.F. Moreau, R. Bataille, S. Minvielle, and Y. Jacques. 1995. Molecular cloning of two isoforms of a receptor for the human hematopoietic cytokine interleukin-11. *Blood.* 86:2534–2540. https://doi.org/10.1182/blood.V86.7.2534.bloodjournal8672534

Dagoneau, N., D. Scheffer, C. Huber, L.I. Al-Gazali, M. Di Rocco, A. Godard, J. Martinovic, A. Raas-Rothschild, S. Sigaudy, S. Unger, et al. 2004. Null leukemia inhibitory factor receptor (LIFR) mutations in Stuve-Wiedemann/Schwartz-Jampel type 2 syndrome. *Am. J. Hum. Genet.* 74:298–305. https://doi.org/10.1086/381715

Davis, S.D., J. Schaller, and R.J. Wedgwood. 1966. Job's Syndrome. Recurrent, "cold", staphylococcal abscesses. *Lancet.* 1:1013–1015. https://doi.org/10.1016/S0140-6736(66)90119-X

de Beaucoudrey, L., A. Puel, O. Filipe-Santos, A. Cobat, P. Ghandil, M. Chrabieh, J. Feinberg, H. von Bernuth, A. Samarina, L. Jannière, et al. 2008. Mutations in STAT3 and IL12RB1 impair the development of human IL-17-producing T cells. *J. Exp. Med.* 205:1543–1550. https://doi.org/10.1084/jem.20080321

Dittrich, E., C.R. Haft, L. Muys, P.C. Heinrich, and L. Graeve. 1996. A dileucine motif and an upstream serine in the interleukin-6 (IL-6) signal transducer gp130 mediate ligand-induced endocytosis and down-regulation of the IL-6 receptor. *J. Biol. Chem.* 271:5487–5494. https://doi.org/10.1074/jbc.271.10.5487

Duncan, C.J.A., S.M.B. Mohamad, D.F. Young, A.J. Skelton, T.R. Leahy, D.C. Munday, K.M. Butler, S. Morfopoulou, J.R. Brown, M. Hubank, et al. 2015. Human IFNAR2 deficiency: Lessons for antiviral immunity. *Sci. Transl. Med.* 7:307ra154. https://doi.org/10.1126/scitranslmed.aac4227

Engelhardt, K.R., S. McGhee, S. Winkler, A. Sassi, C. Woellner, G. Lopez-Herrera, A. Chen, H.S. Kim, M.G. Lloret, I. Schulze, et al. 2009. Large deletions and point mutations involving the dedicator of cytokinesis 8 (DOCK8) in the autosomal-recessive form of hyper-IgE syndrome. *J. Allergy Clin. Immunol.* 124:1289–302.e4. https://doi.org/10.1016/j.jaci.2009.10.038

Erman, B., I. Bilic, T. Hirschmugl, E. Salzer, D. Çagdas, S. Esenboga, Z. Akcoren, O. Sanal, I. Tezcan, and K. Boztug. 2015. Combined immunodeficiency with CD4 lymphopenia and sclerosing cholangitis caused by a novel loss-of-function mutation affecting IL21R. *Haematologica.* 100:e216–e219. https://doi.org/10.3324/haematol.2014.120980

Frey-Jakobs, S., J.M. Hartberger, M. Fliegauf, C. Bossen, M.L. Wehmeyer, J.C. Neubauer, A. Bulashevska, M. Proietti, P. Fröbel, C. Nöltner, et al. 2018. ZNF341 controls STAT3 expression and thereby immunocompetence. *Sci. Immunol.* 3:eaat4941. https://doi.org/10.1126/sciimmunol.aat4941

Fukada, T., M. Hibi, Y. Yamanaka, M. Takahashi-Tezuka, Y. Fujitani, T. Yamaguchi, K. Nakajima, and T. Hirano. 1996. Two signals are necessary for cell proliferation induced by a cytokine receptor gp130: involvement of STAT3 in anti-apoptosis. *Immunity.* 5:449–460. https://doi.org/10.1016/S1074-7613(00)80501-4

Gearing, D.P., M.R. Comeau, D.J. Friend, S.D. Gimpel, C.J. Thut, J. McGourty, K.K. Brasher, J.A. King, S. Gillis, B. Mosley, and A. Et. 1992. The IL-6 signal transducer, gp130: an oncostatin M receptor and affinity converter for the LIF receptor. *Science.* 255:1434–1437. https://doi.org/10.1126/science.1542794

Glocker, E.-O., D. Kotlarz, C. Klein, N. Shah, and B. Grimbacher. 2011. IL-10 and IL-10 receptor defects in humans. *Ann. N. Y. Acad. Sci.* 1246:102–107. https://doi.org/10.1111/j.1749-6632.2011.06339.x

Grimbacher, B., S.M. Holland, J.I. Gallin, F. Greenberg, S.C. Hill, H.L. Malech, J.A. Miller, A.C. O'Connell, and J.M. Puck. 1999a. Hyper-IgE syndrome with recurrent infections--an autosomal dominant multisystem disorder. *N. Engl. J. Med.* 340:692–702. https://doi.org/10.1056/NEJM199903043400904

Grimbacher, B., A.A. Schäffer, S.M. Holland, J. Davis, J.I. Gallin, H.L. Malech, T.P. Atkinson, B.H. Belohradsky, R.H. Buckley, F. Cossu, et al. 1999b. Genetic linkage of hyper-IgE syndrome to chromosome 4. *Am. J. Hum. Genet.* 65:735–744. https://doi.org/10.1086/302547

Hermanns, H.M. 2015. Oncostatin M and interleukin-31: Cytokines, receptors, signal transduction and physiology. *Cytokine Growth Factor Rev.* 26:545–558. https://doi.org/10.1016/j.cytogfr.2015.07.006

Hernandez, N., G. Bucciol, L. Moens, J. Le Pen, M. Shahrooei, E. Goudouris, A. Shirkani, M. Changi-Ashtiani, H. Rokni-Zadeh, E.H. Sayar, et al. 2019. Inherited IFNAR1 deficiency in otherwise healthy patients with adverse reaction to measles and yellow fever live vaccines. *J. Exp. Med.* 216:2057–2070. https://doi.org/10.1084/jem.20182295

Hibi, M., M. Murakami, M. Saito, T. Hirano, T. Taga, and T. Kishimoto. 1990. Molecular cloning and expression of an IL-6 signal transducer, gp130. *Cell.* 63:1149–1157. https://doi.org/10.1016/0092-8674(90)90411-7

Hilton, D.J., A.A. Hilton, A. Raicevic, S. Rakar, M. Harrison-Smith, N.M. Gough, C.G. Begley, D. Metcalf, N.A. Nicola, and T.A. Willson. 1994. Cloning of a murine IL-11 receptor alpha-chain; requirement for gp130 for high affinity binding and signal transduction. *EMBO J.* 13:4765–4775. https://doi.org/10.1002/j.1460-2075.1994.tb06802.x

Holland, S.M., F.R. DeLeo, H.Z. Elloumi, A.P. Hsu, G. Uzel, N. Brodsky, A.F. Freeman, A. Demidowich, J. Davis, M.L. Turner, et al. 2007. STAT3 mutations in the hyper-IgE syndrome. *N. Engl. J. Med.* 357:1608–1619. https://doi.org/10.1056/NEJMoa073687

Hunter, C.A., and S.A. Jones. 2015. IL-6 as a keystone cytokine in health and disease. *Nat. Immunol.* 16:448–457. https://doi.org/10.1038/ni.3153

Itan, Y., L. Shang, B. Boisson, M.J. Ciancanelli, J.G. Markle, R. Martinez-Barricarte, E. Scott, I. Shah, P.D. Stenson, J. Gleeson, et al. 2016. The mutation significance cutoff: gene-level thresholds for variant predictions. *Nat. Methods.* 13:109–110. https://doi.org/10.1038/nmeth.3739

Jouanguy, E., S. Lamhamedi-Cherradi, D. Lammas, S.E. Dorman, M.-C. Fondanèche, S. Dupuis, R. Döffinger, F. Altare, J. Girdlestone, J.-F. Emile, et al. 1999. A human IFNGR1 small deletion hotspot associated with dominant susceptibility to mycobacterial infection. *Nat. Genet.* 21:370–378. https://doi.org/10.1038/7701

Kane, A., E.K. Deenick, C.S. Ma, M.C. Cook, G. Uzel, and S.G. Tangye. 2014. STAT3 is a central regulator of lymphocyte differentiation and function. *Curr. Opin. Immunol.* 28:49–57. https://doi.org/10.1016/j.coi.2014.01.015

Kawasaki, K., Y.-H. Gao, S. Yokose, Y. Kaji, T. Nakamura, T. Suda, K. Yoshida, T. Taga, T. Kishimoto, H. Kataoka, et al. 1997. Osteoclasts are present in gp130-deficient mice. *Endocrinology.* 138:4959–4965. https://doi.org/10.1210/endo.138.11.5534

Khourieh, J., G. Rao, T. Habib, D.T. Avery, A. Lefèvre-Utile, M.-O. Chandesris, A. Belkadi, M. Chrabieh, H. Alwaseem, V. Grandin, et al. 2019. A deep intronic splice mutation of *STAT3* underlies hyper IgE syndrome by negative dominance. *Proc. Natl. Acad. Sci. USA.* 116:16463–16472. https://doi.org/10.1073/pnas.1901409116

Kim, H., T.S. Hawley, R.G. Hawley, and H. Baumann. 1998. Protein tyrosine phosphatase 2 (SHP-2) moderates signaling by gp130 but is not required for the induction of acute-phase plasma protein genes in hepatic cells. *Mol. Cell. Biol.* 18:1525–1533. https://doi.org/10.1128/MCB.18.3.1525

Kircher, M., D.M. Witten, P. Jain, B.J. O'Roak, G.M. Cooper, and J. Shendure. 2014. A general framework for estimating the relative pathogenicity of human genetic variants. *Nat. Genet.* 46:310–315. https://doi.org/10.1038/ng.2892

Kotlarz, D., R. Beier, D. Murugan, J. Diestelhorst, O. Jensen, K. Boztug, D. Pfeifer, H. Kreipe, E.-D. Pfister, U. Baumann, et al. 2012. Loss of

interleukin-10 signaling and infantile inflammatory bowel disease: implications for diagnosis and therapy. *Gastroenterology*. 143:347–355. https://doi.org/10.1053/j.gastro.2012.04.045

Kotlarz, D., N. Ziętara, G. Uzel, T. Weidemann, C.J. Braun, J. Diestelhorst, P.M. Krawitz, P.N. Robinson, J. Hecht, J. Puchałka, et al. 2013. Loss-of-function mutations in the IL-21 receptor gene cause a primary immunodeficiency syndrome. *J. Exp. Med.* 210:433–443. https://doi.org/10.1084/jem.20111229

Kotlarz, D., N. Ziętara, J.D. Milner, and C. Klein. 2014. Human IL-21 and IL-21R deficiencies: two novel entities of primary immunodeficiency. *Curr. Opin. Pediatr.* 26:704–712. https://doi.org/10.1097/MOP.0000000000000160

Kumanogoh, A., S. Marukawa, T. Kumanogoh, H. Hirota, K. Yoshida, I.-S. Lee, T. Yasui, K. Yoshida, T. Taga, and T. Kishimoto. 1997. Impairment of antigen-specific antibody production in transgenic mice expressing a dominant-negative form of gp130. *Proc. Natl. Acad. Sci. USA.* 94: 2478–2482. https://doi.org/10.1073/pnas.94.6.2478

Lehmann, U., J. Schmitz, M. Weissenbach, R.M. Sobota, M. Hörtner, K. Friederichs, I. Behrmann, W. Tsiaris, A. Sasaki, J. Schneider-Mergener, et al. 2003. SHP2 and SOCS3 contribute to Tyr-759-dependent attenuation of interleukin-6 signaling through gp130. *J. Biol. Chem.* 278: 661–671. https://doi.org/10.1074/jbc.M210552200

Li, H., and R. Durbin. 2010. Fast and accurate long-read alignment with Burrows-Wheeler transform. *Bioinformatics.* 26:589–595. https://doi.org/10.1093/bioinformatics/btp698

Li, H., B. Handsaker, A. Wysoker, T. Fennell, J. Ruan, N. Homer, G. Marth, G. Abecasis, and R. Durbin. 1000 Genome Project Data Processing Subgroup. 2009. The Sequence Alignment/Map format and SAMtools. *Bioinformatics.* 25:2078–2079. https://doi.org/10.1093/bioinformatics/btp352

Lütticken, C., U.M. Wegenka, J. Yuan, J. Buschmann, C. Schindler, A. Ziemiecki, A.G. Harpur, A.F. Wilks, K. Yasukawa, T. Taga, and A. Et. 1994. Association of transcription factor APRF and protein kinase Jak1 with the interleukin-6 signal transducer gp130. *Science.* 263:89–92. https://doi.org/10.1126/science.8272872

Ma, C.S., G.Y.J. Chew, N. Simpson, A. Priyadarshi, M. Wong, B. Grimbacher, D.A. Fulcher, S.G. Tangye, and M.C. Cook. 2008. Deficiency of Th17 cells in hyper IgE syndrome due to mutations in STAT3. *J. Exp. Med.* 205: 1551–1557. https://doi.org/10.1084/jem.20080218

Ma, C.S., D.T. Avery, A. Chan, M. Batten, J. Bustamante, S. Boisson-Dupuis, P.D. Arkwright, A.Y. Kreins, D. Averbuch, D. Engelhard, et al. 2012. Functional STAT3 deficiency compromises the generation of human T follicular helper cells. *Blood.* 119:3997–4008. https://doi.org/10.1182/blood-2011-11-392985

Ma, C.S., N. Wong, G. Rao, D.T. Avery, J. Torpy, T. Hambridge, J. Bustamante, S. Okada, J.L. Stoddard, E.K. Deenick, et al. 2015. Monogenic mutations differentially affect the quantity and quality of T follicular helper cells in patients with human primary immunodeficiencies. *J. Allergy Clin. Immunol.* 136:993–1006.e1. https://doi.org/10.1016/j.jaci.2015.05.036

Ma, C.S., N. Wong, G. Rao, A. Nguyen, D.T. Avery, K. Payne, J. Torpy, P. O'Young, E. Deenick, J. Bustamante, et al. 2016. Unique and shared signaling pathways cooperate to regulate the differentiation of human CD4+ T cells into distinct effector subsets. *J. Exp. Med.* 213:1589–1608. https://doi.org/10.1084/jem.20151467

Ma, C.A., J.R. Stinson, Y. Zhang, J.K. Abbott, M.A. Weinreich, P.J. Hauk, P.R. Reynolds, J.J. Lyons, C.G. Nelson, E. Ruffo, et al. 2017. Germline hypomorphic *CARD11* mutations in severe atopic disease. *Nat. Genet.* 49: 1192–1201. https://doi.org/10.1038/ng.3898

Martínez-Barricarte, R., J.G. Markle, C.S. Ma, E.K. Deenick, N. Ramírez-Alejo, F. Mele, D. Latorre, S.A. Mahdaviani, C. Aytekin, D. Mansouri, et al. 2018. Human IFN-γ immunity to mycobacteria is governed by both IL-12 and IL-23. *Sci. Immunol.* 3:eaau6759. https://doi.org/10.1126/sciimmunol.aau6759

McKenna, A., M. Hanna, E. Banks, A. Sivachenko, K. Cibulskis, A. Kernytsky, K. Garimella, D. Altshuler, S. Gabriel, M. Daly, and M.A. DePristo. 2010. The Genome Analysis Toolkit: a MapReduce framework for analyzing next-generation DNA sequencing data. *Genome Res.* 20:1297–1303. https://doi.org/10.1101/gr.107524.110

Mikelonis, D., C.L. Jorcyk, K. Tawara, and J.T. Oxford. 2014. Stüve-Wiedemann syndrome: LIFR and associated cytokines in clinical course and etiology. *Orphanet J. Rare Dis.* 9:34. https://doi.org/10.1186/1750-1172-9-34

Milner, J.D., J.M. Brenchley, A. Laurence, A.F. Freeman, B.J. Hill, K.M. Elias, Y. Kanno, C. Spalding, H.Z. Elloumi, M.L. Paulson, et al. 2008. Impaired T(H) 17 cell differentiation in subjects with autosomal dominant hyper-IgE syndrome. *Nature.* 452:773–776. https://doi.org/10.1038/nature06764

Minegishi, Y., M. Saito, S. Tsuchiya, I. Tsuge, H. Takada, T. Hara, N. Kawamura, T. Ariga, S. Pasic, O. Stojkovic, et al. 2007. Dominant-negative mutations in the DNA-binding domain of STAT3 cause hyper-IgE syndrome. *Nature.* 448:1058–1062. https://doi.org/10.1038/nature06096

Monies, D., M. Abouelhoda, M. Assoum, N. Moghrabi, R. Rafiullah, N. Almontashiri, M. Alowain, H. Alzaidan, M. Alsayed, S. Subhani, et al. 2019. Lessons Learned from Large-Scale, First-Tier Clinical Exome Sequencing in a Highly Consanguineous Population. *Am. J. Hum. Genet.* 104:1182–1201. https://doi.org/10.1016/j.ajhg.2019.04.011

Moran, C.J., T.D. Walters, C.-H. Guo, S. Kugathasan, C. Klein, D. Turner, V.M. Wolters, R.H. Bandsma, M. Mouzaki, M. Zachos, et al. 2013. IL-10R polymorphisms are associated with very-early-onset ulcerative colitis. *Inflamm. Bowel Dis.* 19:115–123. https://doi.org/10.1002/ibd.22974

Mosley, B., C. De Imus, D. Friend, N. Boiani, B. Thoma, L.S. Park, and D. Cosman. 1996. Dual oncostatin M (OSM) receptors. Cloning and characterization of an alternative signaling subunit conferring OSM-specific receptor activation. *J. Biol. Chem.* 271:32635–32643. https://doi.org/10.1074/jbc.271.51.32635

Murakami, M., M. Hibi, N. Nakagawa, T. Nakagawa, K. Yasukawa, K. Yamanishi, T. Taga, and T. Kishimoto. 1993. IL-6-induced homodimerization of gp130 and associated activation of a tyrosine kinase. *Science.* 260:1808–1810. https://doi.org/10.1126/science.8511589

Murakami, M., D. Kamimura, and T. Hirano. 2019. Pleiotropy and Specificity: Insights from the Interleukin 6 Family of Cytokines. *Immunity.* 50: 812–831. https://doi.org/10.1016/j.immuni.2019.03.027

Nakajima, K., Y. Yamanaka, K. Nakae, H. Kojima, M. Ichiba, N. Kiuchi, T. Kitaoka, T. Fukada, M. Hibi, and T. Hirano. 1996. A central role for Stat3 in IL-6-induced regulation of growth and differentiation in M1 leukemia cells. *EMBO J.* 15:3651–3658. https://doi.org/10.1002/j.1460-2075.1996.tb00734.x

Ng, P.C., and S. Henikoff. 2001. Predicting deleterious amino acid substitutions. *Genome Res.* 11:863–874. https://doi.org/10.1101/gr.176601

Nicholson, S.E., D. De Souza, L.J. Fabri, J. Corbin, T.A. Willson, J.-G. Zhang, A. Silva, M. Asimakis, A. Farley, A.D. Nash, et al. 2000. Suppressor of cytokine signaling-3 preferentially binds to the SHP-2-binding site on the shared cytokine receptor subunit gp130. *Proc. Natl. Acad. Sci. USA.* 97:6493–6498. https://doi.org/10.1073/pnas.100135197

Nicola, N.A., and J.J. Babon. 2015. Leukemia inhibitory factor (LIF). *Cytokine Growth Factor Rev.* 26:533–544. https://doi.org/10.1016/j.cytogfr.2015.07.001

Nieminen, P., N.V. Morgan, A.L. Fenwick, S. Parmanen, L. Veistinen, M.L. Mikkola, P.J. van der Spek, A. Giraud, L. Judd, S. Arte, et al. 2011. Inactivation of IL11 signaling causes craniosynostosis, delayed tooth eruption, and supernumerary teeth. *Am. J. Hum. Genet.* 89:67–81. https://doi.org/10.1016/j.ajhg.2011.05.024

Ohtani, T., K. Ishihara, T. Atsumi, K. Nishida, Y. Kaneko, T. Miyata, S. Itoh, M. Narimatsu, H. Maeda, T. Fukada, et al. 2000. Dissection of signaling cascades through gp130 in vivo: reciprocal roles for STAT3- and SHP2-mediated signals in immune responses. *Immunity.* 12:95–105. https://doi.org/10.1016/S1074-7613(00)80162-4

Pflanz, S., L. Hibbert, J. Mattson, R. Rosales, E. Vaisberg, J.F. Bazan, J.H. Phillips, T.K. McClanahan, R. de Waal Malefyt, and R.A. Kastelein. 2004. WSX-1 and glycoprotein 130 constitute a signal-transducing receptor for IL-27. *J. Immunol.* 172:2225–2231. https://doi.org/10.4049/jimmunol.172.4.2225

Puel, A., and J.-L. Casanova. 2019. The nature of human IL-6. *J. Exp. Med.* 216: 1969–1971. https://doi.org/10.1084/jem.20191002

Puel, A., S. Cypowyj, J. Bustamante, J.F. Wright, L. Liu, H.K. Lim, M. Migaud, L. Israel, M. Chrabieh, M. Audry, et al. 2011. Chronic mucocutaneous candidiasis in humans with inborn errors of interleukin-17 immunity. *Science.* 332:65–68. https://doi.org/10.1126/science.1200439

Renner, E.D., T.R. Torgerson, S. Rylaarsdam, S. Añover-Sombke, K. Golob, T. LaFlam, Q. Zhu, and H.D. Ochs. 2007. STAT3 mutation in the original patient with Job's syndrome. *N. Engl. J. Med.* 357:1667–1668. https://doi.org/10.1056/NEJMc076367

Rose-John, S. 2018. Interleukin-6 Family Cytokines. *Cold Spring Harb. Perspect. Biol.* 10:a028415. https://doi.org/10.1101/cshperspect.a028415

Saçilanateş, B., F. Doğu, M. Özkan, N. Akay, A. İkincioğullari, and H. Akay. 2005. Giant bullae of the lung treated successfully by surgery in a patient with Hyper-IgE Syndrome (Job's). *J Ankara Univ Fac Med.* 58:15–17.

Salzer, E., A. Kansu, H. Sic, P. Májek, A. Ikincioğullari, F.E. Dogu, N.K. Prengemann, E. Santos-Valente, W.F. Pickl, I. Bilic, et al. 2014. Early-onset inflammatory bowel disease and common variable immunodeficiency-like disease caused by IL-21 deficiency. *J. Allergy Clin. Immunol.* 133: 1651–9.e12. https://doi.org/10.1016/j.jaci.2014.02.034

Sassi, A., S. Lazaroski, G. Wu, S.M. Haslam, M. Fliegauf, F. Mellouli, T. Patiroglu, E. Unal, M.A. Ozdemir, Z. Jouhadi, et al. 2014. Hypomorphic homozygous mutations in phosphoglucomutase 3 (PGM3) impair immunity and increase serum IgE levels. *J. Allergy Clin. Immunol.* 133: 1410–1419: 1419.e1–1419.e13. https://doi.org/10.1016/j.jaci.2014.02.025

Schaper, F., C. Gendo, M. Eck, J. Schmitz, C. Grimm, D. Anhuf, I.M. Kerr, and P.C. Heinrich. 1998. Activation of the protein tyrosine phosphatase SHP2 via the interleukin-6 signal transducing receptor protein gp130 requires tyrosine kinase Jak1 and limits acute-phase protein expression. *Biochem. J.* 335:557–565. https://doi.org/10.1042/bj3350557

Schmitz, J., M. Weissenbach, S. Haan, P.C. Heinrich, and F. Schaper. 2000. SOCS3 exerts its inhibitory function on interleukin-6 signal transduction through the SHP2 recruitment site of gp130. *J. Biol. Chem.* 275: 12848–12856. https://doi.org/10.1074/jbc.275.17.12848

Schwerd, T., S.R.F. Twigg, D. Aschenbrenner, S. Manrique, K.A. Miller, I.B. Taylor, M. Capitani, S.J. McGowan, E. Sweeney, A. Weber, et al. 2017. A biallelic mutation in *IL6ST* encoding the GP130 co-receptor causes immunodeficiency and craniosynostosis. *J. Exp. Med.* 214:2547–2562. https://doi.org/10.1084/jem.20161810

Selander, K.S., L. Li, L. Watson, M. Merrell, H. Dahmen, P.C. Heinrich, G. Müller-Newen, and K.W. Harris. 2004. Inhibition of gp130 signaling in breast cancer blocks constitutive activation of Stat3 and inhibits in vivo malignancy. *Cancer Res.* 64:6924–6933. https://doi.org/10.1158/0008-5472.CAN-03-2516

Shahin, T., D. Aschenbrenner, D. Cagdas, S.K. Bal, C.D. Conde, W. Garncarz, D. Medgyesi, T. Schwerd, B. Karaatmaca, P.G. Cetinkaya, et al. 2019. Selective loss of function variants in *IL6ST* cause Hyper-IgE syndrome with distinct impairments of T-cell phenotype and function. *Haematologica.* 104:609–621. https://doi.org/10.3324/haematol.2018.194233

Siegel, A.M., J. Heimall, A.F. Freeman, A.P. Hsu, E. Brittain, J.M. Brenchley, D.C. Douek, G.H. Fahle, J.I. Cohen, S.M. Holland, and J.D. Milner. 2011. A critical role for STAT3 transcription factor signaling in the development and maintenance of human T cell memory. *Immunity.* 35:806–818. https://doi.org/10.1016/j.immuni.2011.09.016

Spencer, S., S. Köstel Bal, W. Egner, H. Lango Allen, S.I. Raza, C.A. Ma, M. Gürel, Y. Zhang, G. Sun, R.A. Sabroe, et al. 2019. Loss of the interleukin-6 receptor causes immunodeficiency, atopy, and abnormal inflammatory responses. *J. Exp. Med.* 216:1986–1998. https://doi.org/10.1084/jem.20190344

Stahl, N., T.J. Farruggella, T.G. Boulton, Z. Zhong, J.E. Darnell Jr., and G.D. Yancopoulos. 1995. Choice of STATs and other substrates specified by modular tyrosine-based motifs in cytokine receptors. *Science.* 267: 1349–1353. https://doi.org/10.1126/science.7871433

Stepensky, P., B. Keller, O. Abuzaitoun, A. Shaag, B. Yaacov, S. Unger, M. Seidl, M. Rizzi, M. Weintraub, O. Elpeleg, and K. Warnatz. 2015. Extending the clinical and immunological phenotype of human interleukin-21 receptor deficiency. *Haematologica.* 100:e72–e76. https://doi.org/10.3324/haematol.2014.112508

Steward-Tharp, S.M., A. Laurence, Y. Kanno, A. Kotlyar, A.V. Villarino, G. Sciume, S. Kuchen, W. Resch, E.A. Wohlfert, K. Jiang, et al. 2014. A mouse model of HIES reveals pro- and anti-inflammatory functions of STAT3. *Blood.* 123:2978–2987. https://doi.org/10.1182/blood-2013-09-523167

Symes, A., N. Stahl, S.A. Reeves, T. Farruggella, T. Servidei, T. Gearan, G. Yancopoulos, and J.S. Fink. 1997. The protein tyrosine phosphatase SHP-2 negatively regulates ciliary neurotrophic factor induction of gene expression. *Curr. Biol.* 7:697–700. https://doi.org/10.1016/S0960-9822(06)00298-3

Taga, T., M. Hibi, Y. Hirata, K. Yamasaki, K. Yasukawa, T. Matsuda, T. Hirano, and T. Kishimoto. 1989. Interleukin-6 triggers the association of its receptor with a possible signal transducer, gp130. *Cell.* 58:573–581. https://doi.org/10.1016/0092-8674(89)90438-8

Takeda, K., K. Noguchi, W. Shi, T. Tanaka, M. Matsumoto, N. Yoshida, T. Kishimoto, and S. Akira. 1997. Targeted disruption of the mouse Stat3 gene leads to early embryonic lethality. *Proc. Natl. Acad. Sci. USA.* 94: 3801–3804. https://doi.org/10.1073/pnas.94.8.3801

Vogel, T.P., J.D. Milner, and M.A. Cooper. 2015. The Ying and Yang of STAT3 in Human Disease. *J. Clin. Immunol.* 35:615–623. https://doi.org/10.1007/s10875-015-0187-8

Waetzig, G.H., A. Chalaris, P. Rosenstiel, J. Suthaus, C. Holland, N. Karl, L. Vallés Uriarte, A. Till, J. Scheller, J. Grötzinger, et al. 2010. N-linked glycosylation is essential for the stability but not the signaling function of the interleukin-6 signal transducer glycoprotein 130. *J. Biol. Chem.* 285:1781–1789. https://doi.org/10.1074/jbc.M109.075952

Wilson, R.P., M.L. Ives, G. Rao, A. Lau, K. Payne, M. Kobayashi, P.D. Arkwright, J. Peake, M. Wong, S. Adelstein, et al. 2015. STAT3 is a critical cell-intrinsic regulator of human unconventional T cell numbers and function. *J. Exp. Med.* 212:855–864. https://doi.org/10.1084/jem.20141992

Yamanaka, Y., K. Nakajima, T. Fukada, M. Hibi, and T. Hirano. 1996. Differentiation and growth arrest signals are generated through the cytoplasmic region of gp130 that is essential for Stat3 activation. *EMBO J.* 15:1557–1565. https://doi.org/10.1002/j.1460-2075.1996.tb00500.x

Yamasaki, K., T. Taga, Y. Hirata, H. Yawata, Y. Kawanishi, B. Seed, T. Taniguchi, T. Hirano, and T. Kishimoto. 1988. Cloning and expression of the human interleukin-6 (BSF-2/IFN beta 2) receptor. *Science.* 241:825–828. https://doi.org/10.1126/science.3136546

Yoshida, K., T. Taga, M. Saito, S. Suematsu, A. Kumanogoh, T. Tanaka, H. Fujiwara, M. Hirata, T. Yamagami, T. Nakahata, et al. 1996. Targeted disruption of gp130, a common signal transducer for the interleukin 6 family of cytokines, leads to myocardial and hematological disorders. *Proc. Natl. Acad. Sci. USA.* 93:407–411. https://doi.org/10.1073/pnas.93.1.407

Zhang, Q., J.C. Davis, I.T. Lamborn, A.F. Freeman, H. Jing, A.J. Favreau, H.F. Matthews, J. Davis, M.L. Turner, G. Uzel, et al. 2009. Combined immunodeficiency associated with DOCK8 mutations. *N. Engl. J. Med.* 361: 2046–2055. https://doi.org/10.1056/NEJMoa0905506

Zhang, Y., X. Yu, M. Ichikawa, J.J. Lyons, S. Datta, I.T. Lamborn, H. Jing, E.S. Kim, M. Biancalana, L.A. Wolfe, et al. 2014. Autosomal recessive phosphoglucomutase 3 (PGM3) mutations link glycosylation defects to atopy, immune deficiency, autoimmunity, and neurocognitive impairment. *J. Allergy Clin. Immunol.* 133:1400–1409: 1409.e1–1409.e5. https://doi.org/10.1016/j.jaci.2014.02.013

Zhang, P., B. Bigio, F. Rapaport, S.-Y. Zhang, J.-L. Casanova, L. Abel, B. Boisson, and Y. Itan. 2018a. PopViz: a webserver for visualizing minor allele frequencies and damage prediction scores of human genetic variations. *Bioinformatics.* 34:4307–4309. https://doi.org/10.1093/bioinformatics/bty536

Zhang, Q., B. Boisson, V. Béziat, A. Puel, and J.-L. Casanova. 2018b. Human hyper-IgE syndrome: singular or plural? *Mamm. Genome.* 29:603–617. https://doi.org/10.1007/s00335-018-9767-2

JEM

# Supplemental material

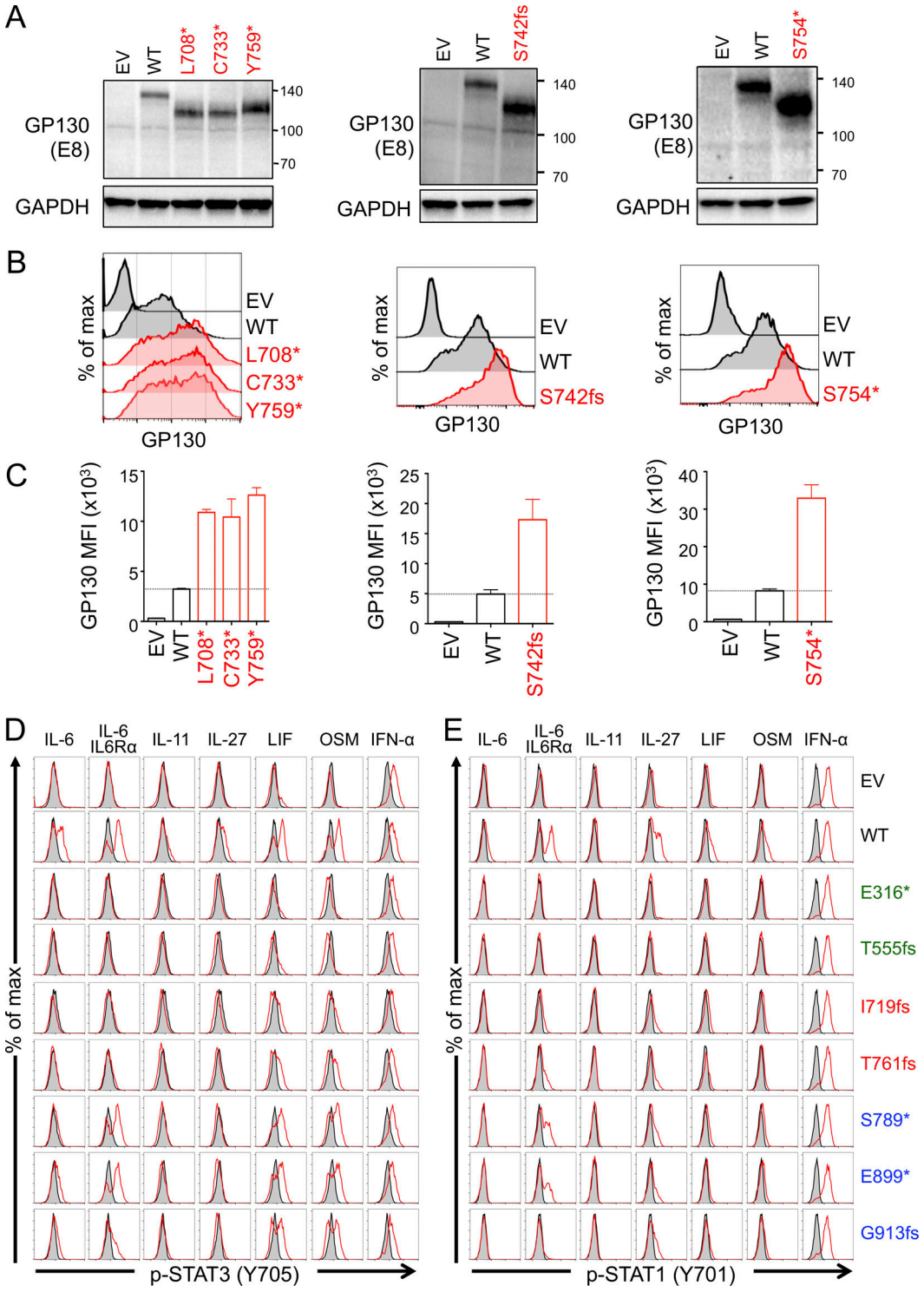


Figure S1. **Expression of the GP130 mutants and phosphorylation assays of STAT1 and STAT3. (A)** GP130-deficient HEK293T cells were transfected with an empty pCMV6 plasmid (EV) or with pCMV6 plasmids encoding the WT, L708*, C733*, S742fs, S754*, or Y759* GP130 mutants. Total protein was extracted and subjected to immunoblotting with a mAb against GP130 (amino acids 365–619, clone E8). GAPDH was used as a loading control. Western blots representative of three independent experiments are shown. **(B and C)** GP130-deficient HEK293T cells were transfected as described in A. After 48 h, the cells were harvested, stained for extracellular GP130, and analyzed by flow cytometry. Representative staining (B) and a recapitulative graph of GP130 mean fluorescence intensity (C) are shown. The bars and error bars represent the mean of three independent experiments and the standard deviation, respectively. **(D and E)** GP130-deficient HEK293T cells were transfected with an empty pCMV6 plasmid (EV) or with pCMV6 plasmids encoding the WT, or E316*, T555fs, L708*, I719fs, C733*, S742fs, S754*, Y759*, T761fs, S789*, E899*, G913fs GP130 mutants. After 24 h of incubation, the cells were stimulated for 15 min with the indicated GP130-dependent cytokines (red line) or left unstimulated (black line), and the phosphorylation of STAT3 (pY705; D) and STAT1 (pY701; E) was then evaluated by flow cytometry. The results obtained with the I719fs and T761fs mutants are representative of the results obtained with the other mutants found in HIES patients (L708*, C733*, S742fs, S754*, and Y759*). Representative results from three independent experiments are shown.

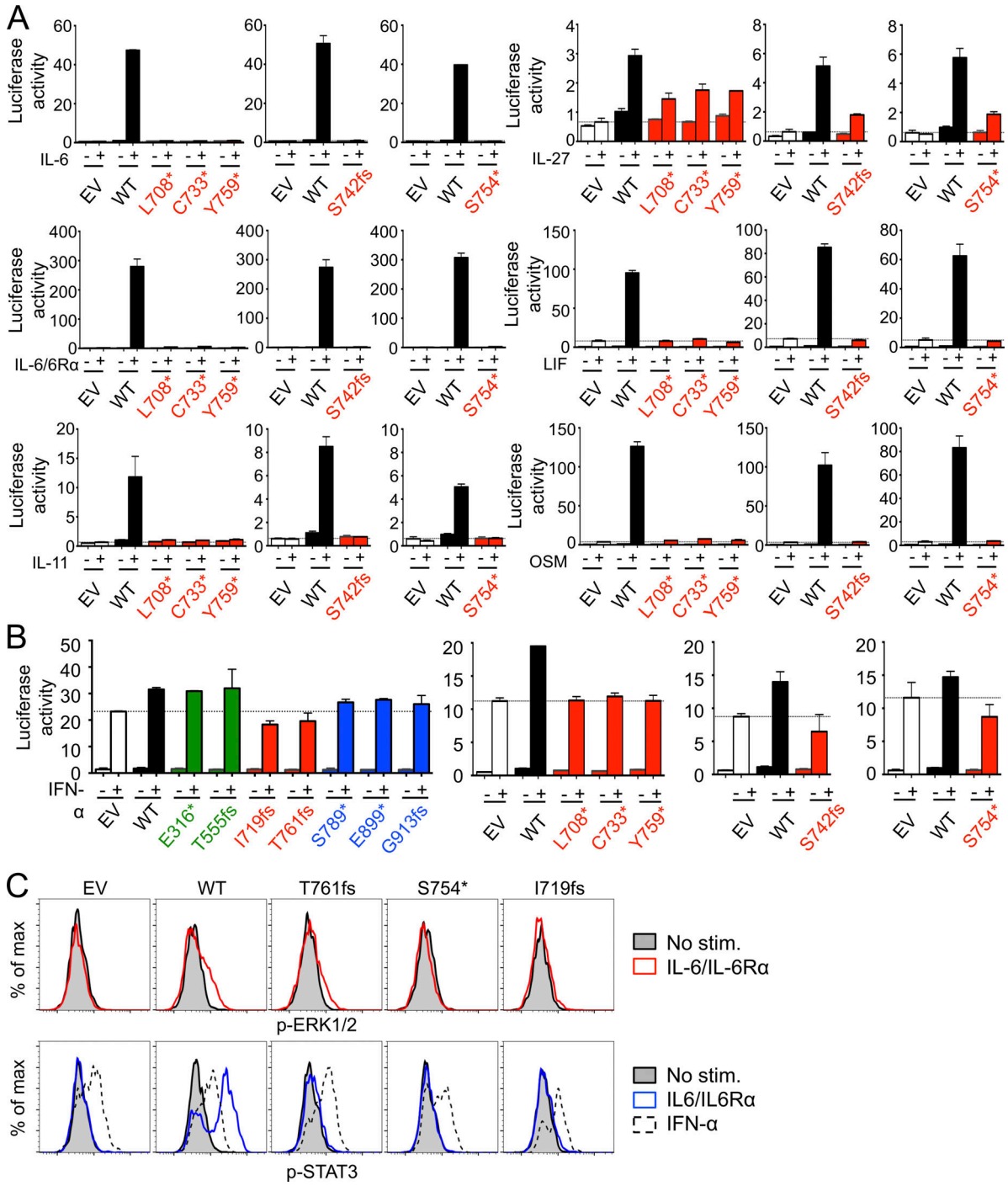


Figure S2. **Molecular characterization of the GP130 mutants. (A)** STAT3 activity, as assessed in a luciferase assay. GP130-deficient HEK293T cells transfected with an empty pCMV6 vector (EV) or with a plasmid encoding the WT or the indicated GP130 mutant plus a pGL4.47 reporter plasmid carrying the luciferase cDNA downstream from five SIEs. Cells were stimulated with the indicated cytokine (+), 24 h after transfection, or were left unstimulated (–) for another 24 h before the measurement of luciferase activity. The horizontal dotted line indicates the luciferase activity after the stimulation, with the indicated cytokine, of cells transfected with the empty pCMV6 vector. The results shown are the mean and standard error of the mean for a technical duplicate. A luciferase assay representative of two independent experiments is shown. **(B)** STAT3 activity, as assessed in a luciferase assay, after IFN-α stimulation. GP130-deficient HEK293T cells were transfected as described in A. Cells were stimulated with IFN-α (+), 24 h after transfection, or were left unstimulated (–) for another 24 h before the measurement of luciferase activity. The horizontal dotted line indicates the luciferase activity after the stimulation, with the indicated cytokine, of cells transfected with the empty pCMV6 vector. The results shown are the mean and standard error of the mean for a technical duplicate. A luciferase assay representative of two or three independent experiments is shown. **(C)** GP130-deficient HEK293T cells were transfected with an empty pCMV6 plasmid (EV) or with pCMV6 plasmids encoding the WT or I719fs, S754*, and T761fs GP130 mutants. After 24 h of incubation, the cells were starved of serum for 16 h and then stimulated for 15 min with the indicated GP130-dependent cytokines or left unstimulated, and the phosphorylation of ERK1/2 (pT202/pY204; top panel) or STAT3 (Y705, positive control; lower panel) was evaluated by flow cytometry. Representative results from two independent experiments are shown.

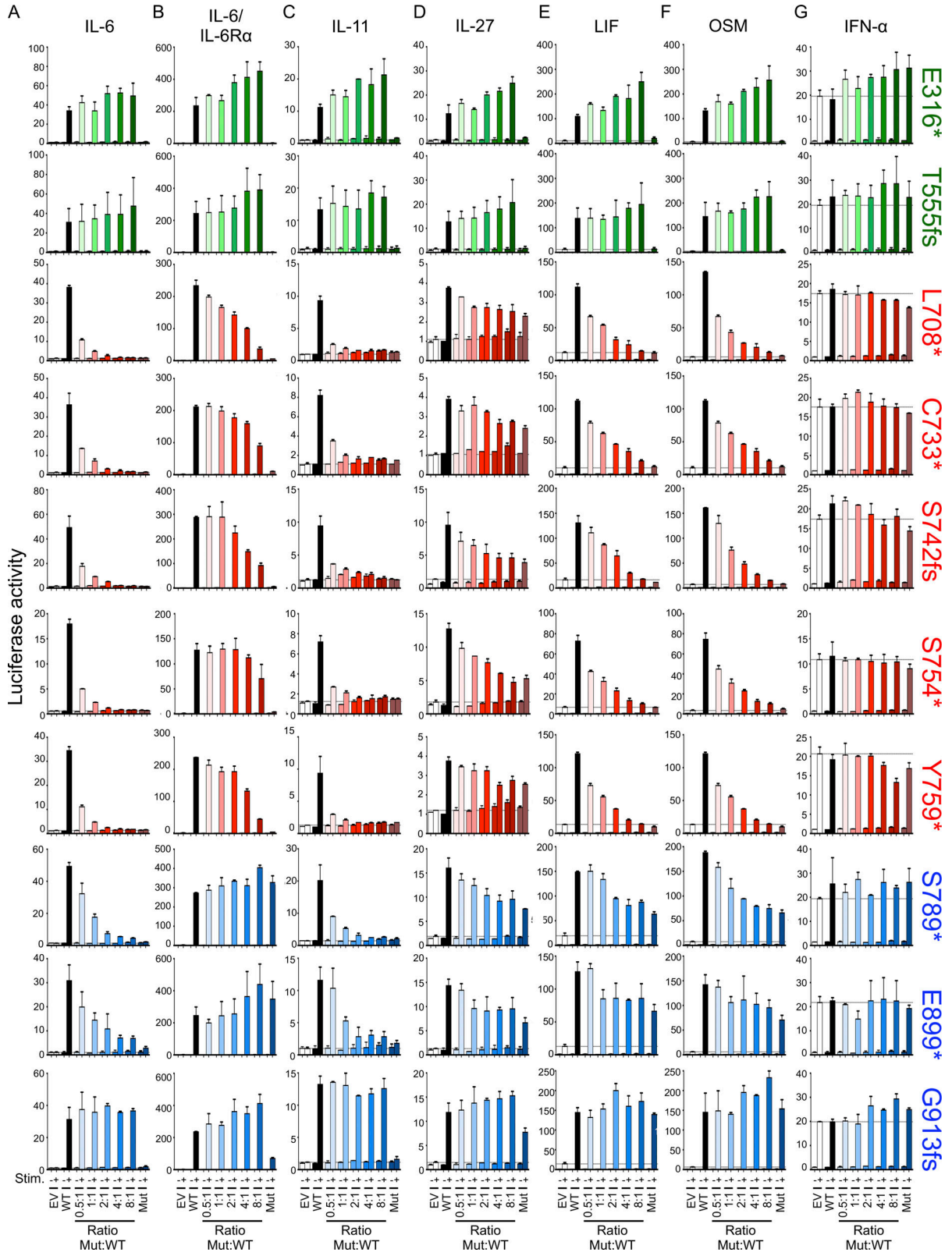


Figure S3. **Assay of the negative dominance of the GP130 mutants. (A–G)** GP130-deficient HEK293T cells transfected with an empty pCMV6 vector or a vector encoding the WT GP130 (25 ng) and various amounts (25–200 ng) of pCMV6 vector encoding the indicated GP130 mutant (Mut) plus a pGL4.47 reporter plasmid carrying the luciferase cDNA downstream of five SIEs. GP130-deficient HEK293T cells transfected with only the WT (25 ng) or the mutant GP130 (200 ng) were used as controls. Cells were stimulated with the indicated cytokine 24 h after transfection or were left unstimulated for another 24 h before the measurement of luciferase activity. The results shown are the mean and standard error of the mean for a technical duplicate. Luciferase assays representative of two independent experiments are shown.

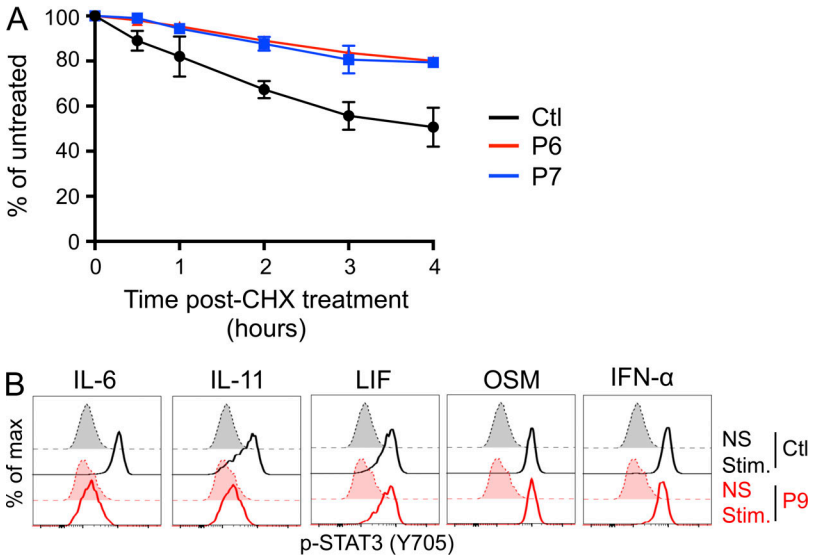


Figure S4. **Primary fibroblasts. (A)** Kinetics of GP130 degradation. Primary fibroblasts from P6, P7, and one healthy control were incubated for the times indicated (30 min to 4 h) with cycloheximide (CHX) to inhibit protein synthesis. GP130 levels were then evaluated by flow cytometry. The expression levels shown are normalized relative to the nonstimulated time point (100%). The means and standard errors of the means from three independent experiments are shown. **(B)** p-STAT3 in P9. Primary fibroblasts from P9 and one healthy control (Ctl) were stimulated (Stim) for 15 min with IL-6, IL-11, LIF, OSM, and IFN-α or left unstimulated (NS), and the phosphorylation of STAT3 (pY705) was then evaluated by flow cytometry.

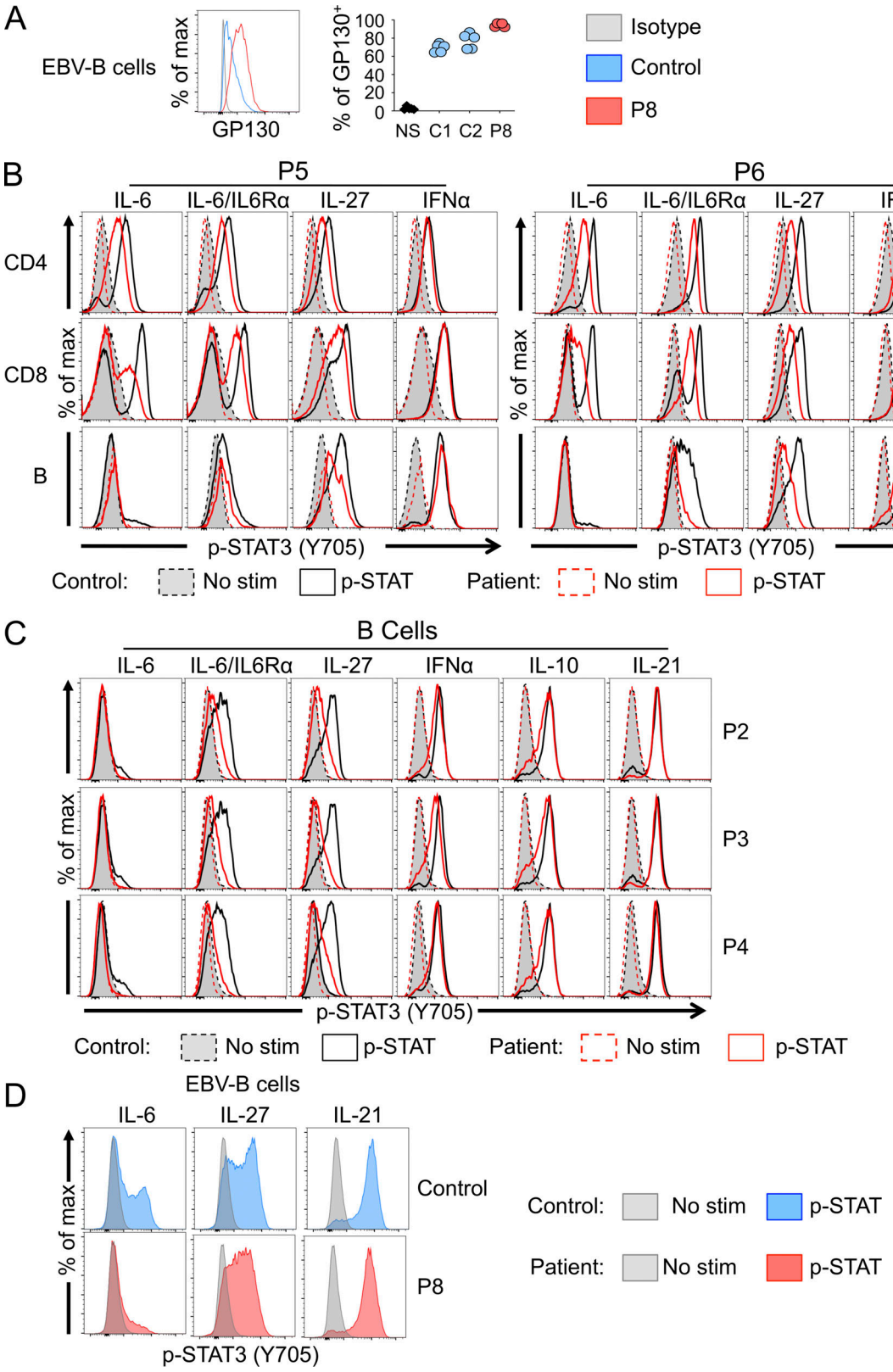


Figure S5. **GP130 expression and function in PBMCs. (A)** GP130 levels in EBV-B cell lines from two controls (C1 and C2) and P8. Representative data are shown on the left and are summarized in a graph on the right. **(B)** PBMCs from P5 (red lines, left plots), P6 (red lines, right plots), and two controls (black lines) were stimulated for 15 min with IL-6, IL-6/IL-6Rα, IL-27, or IFN-α or left unstimulated, and the phosphorylation of STAT3 (pY705) was then evaluated in the indicated subsets. **(C)** PBMCs of P2-P4 (red lines) and controls (black lines) were stimulated for 15 min with IL-6, IL-6/IL-6Rα, IL-27, IFN-α, IL-10, or IL-21 or left unstimulated, and the phosphorylation of STAT3 (pY705) was then evaluated in B cells. **(D)** EBV-B cell lines from P8 and a control were stimulated for 15 min with IL-6, IL-27, or IL-21 or left unstimulated, and the phosphorylation of STAT3 (pY705) was then evaluated.

**Table S1 is a clinical summary of IL6ST-DN patients. Table S2 lists the biological parameters of patients with DN *IL6ST* mutations. Table S3 lists the biological parameters of patients with DN *IL6ST* mutations. Data S1 lists members of the Undiagnosed Diseases Network.**